AD $\#$-/08292

TECHNICAL REPORT ARBRL-TR-02380

THE EFFECTS OF PROPELLANT BURN ON THE SURFACE COMPOSITION OF GUN STEEL

A. Niiler
R. Birkmire
S. E. Caldwell

November 1981

US ARMY ARMAMENT RESEARCH AND DEVELOPMENT COMMAND
BALLISTIC RESEARCH LABORATORY
ABERDEEN PROVING GROUND, MARYLAND

REPORT DOCUMENTATION PAGE		READ INSTRUCTIONS BEFORE COMPLETING FORM
1. REPORT NUMBER TECHNICAL REPORT ARBRL-TR-02380	2. GOVT ACCESSION NO.	3. RECIPIENT'S CATALOG NUMBER
4. TITLE *(and Subtitle)* The Effects of Propellant Burn on the Surface Composition of Gun Steel		5. TYPE OF REPORT & PERIOD COVERED
		6. PERFORMING ORG. REPORT NUMBER
7. AUTHOR(s) A. Niiler, R. Birkmire and S.E. Caldwell		8. CONTRACT OR GRANT NUMBER(s)
9. PERFORMING ORGANIZATION NAME AND ADDRESS Ballistic Research Laboratory ATTN: DRDAR-BLB Aberdeen Proving Ground, MD 21005		10. PROGRAM ELEMENT, PROJECT, TASK AREA & WORK UNIT NUMBERS 1L162618AH80
11. CONTROLLING OFFICE NAME AND ADDRESS US Army Armament Research & Development Command Ballistic Research Laboratory ATTN: DRDAR-BL, APG, MD 21005		12. REPORT DATE November 1981
		13. NUMBER OF PAGES 71
14. MONITORING AGENCY NAME & ADDRESS*(if different from Controlling Office)*		15. SECURITY CLASS. *(of this report)* UNCLASSIFIED
		15e. DECLASSIFICATION/DOWNGRADING SCHEDULE

16. DISTRIBUTION STATEMENT *(of this Report)*

Approved for public release; distribution unlimited.

17. DISTRIBUTION STATEMENT *(of the abstract entered in Block 20, if different from Report)*

18. SUPPLEMENTARY NOTES

19. KEY WORDS *(Continue on reverse side if necessary and identify by block number)*

Erosion, Gun Tube Erosion, Thermo-chemical Erosion, Surface Analysis, Ion Beam Analysis

20. ABSTRACT *(Continue on reverse side if necessary and identify by block number)* (hmn)

The erosion of gun barrel bore surfaces caused by high temperature, high pressure and high velocity gases is responsible for the lives of many such barrels being wear-limited. In addition, such interactions are often accompanied by significant alterations to the remaining bore surfaces. An ion beam analysis method has been used to characterize the depths and compositions of the outer, sub-micron layers of gun steel surfaces that have been exposed to a variety of environments from several propellant/additive combinations. Correlations be-

tween the oxide/nitride concentrations in the surface layers, the propellant flame temperatures and erosive wear obtained. Scanning electron microscope observations of exposed surfaces were also made. The combined results indicate the presence of thermo-chemical erosion as well as erosion by a surface melt and wipe-off process.

TABLE OF CONTENTS

LIST OF FIGURES

1. INTRODUCTION

During the course of the erosion of a gun tube bore surface by the combustion products of burning propellants, significant alterations to that surface are caused by the interaction between the metal and the hot gases at high pressures. After only a small number of exposures, physical and metallurgical changes to the surface are manifested by the appearance of cracking along the grain boundaries and a heat affected region known as the "white" layer[1]. The surface most likely undergoes the austentite/martensite transformation with each exposure causing volume changes which result in heat checking and deep cracking after many exposures[1]. In many cases flow patterns are observed, indicating that the surface melts and then is sheared by the flowing gases[2,3]. In addition to the metallurgical and physical changes taking place, one can also expect to find chemical effects which are present only in the surface layers. These effects are due to chemical reactions between the combustion products and the metal at the surface and/or physical effects such as enhanced diffusion along grain boundaries. Although gross changes have been well documented through the use of instruments such as Scanning Electron Microscopes (SEM), borescopes, hardness testers, and a variety of other metallurgical methods, the instrumentation and techniques capable of measuring the chemical changes on the surface have only been applied recently. Techniques such as X-ray Photoelectron Spectroscopy (XPS), Characteristic X-ray Analyses and Ion Beam Analysis (IBA) are now being applied to the study of gun bore surfaces.

To date, most experiments on the effects of erosion on gun steel have been done in tests where large numbers of rounds have been fired through a barrel. Afterwards, the bore surface was destructively examined. In such experiments, gross effects such as heat checking, fatigue cracking and in cases where additives are used, barrel fouling may obliterate many of the details of the erosion process. A method by which the outer surface layers of a steel sample exposed to the erosive effects of burning propellants can be examined between consecutive shots would be very useful. Since in a typical large caliber gun the erosive wear amounts to about 1 μm per shot, it is highly probable that

1. Sidney Breitbart, "On the Erosion of Metallic Nozzles by Powder Gases," Ballistic Research Laboratory Memorandum Report No. 533, April 1951. AD #802148
2. Franklin A. Vassalo and W. Richard Brown, "Shock Tube Gun Melting Erosion Study," Contract Report, ARBRL-CR-00406, August 1979. AD #A076219
3. A.C. Alkidas, S.O. Morris, C.W. Christoe, L.H. Caveny, and M. Summerfield, "Erosive Effects of Various Pure and Combustion-Generated Gases on Metals, Part II," Contract Report, AMMRC CTR 77-25, October 1977.

such individual shots affect a surface layer of approximately the same thickness. Thus, this surface analysis method must be capable of examining that outer 1 μm layer of the steel.

At the BRL, a surface analysis technique employing ion beams has been developed which is capable of quantitative measurement of the concentrations and depth profiles of carbon, nitrogen and oxygen in the outer micron layers of eroded samples. These elements are of greatest interest because their compounds constitute a large percentage of a given propellant. As the propellant combustion products interact with the steel surface, they either melt the surface and blow it away or change the surface layer compositions. When additives are used, interactions may also occur between the hot propellant gases at high temperatures and the additive compounds. This raises the possibility that the heated surface acts either as a catalyst or condenser of the gaseous products. A measure of the carbon, nitrogen and oxygen concentrations left behind and the depth profile of the affected layer in the steel surface can be expected to yield detailed information about the nature of the processes involved between the hot gases and the surface during the propellant burn.

A number of experiments[1,4,5] have indicated that erosion reduction may, in part, be due to the formation of protective layers on the steel surface which are often quite thin. These layers, of different physical and chemical composition than the substrate steel, protect that steel by reducing the flow of heat to the steel[6]. The characteristics of such protective layers, the conditions under which they form and other details needed for their optimization are not understood. In addition, although the erosion reducing properties of propellant additives such as TiO_2 wax have long been appreciated, the detailed mechanisms by which these additives work have not been clearly described. For a complete review of efforts to reduce gun tube erosion by the use of high temperature metal coatings as well as various wear reducing additives, see the Proceedings of the Tri-Service Gun Tube Wear and Erosion Symposium.[7]

4.   J. Richard Ward and Timothy L. Brosseau, "Role of the Insulating Layer From TiO_2-Wax Liner in Reducing Gun Tube Wear," Ballistic Research Laboratory Technical Report ARBRL-TR-02238, April 1980.
5.   R. Birkmire and A. Niiler, "Applications of the Radioisotope Wear Measurement Technique," Ballistic Research Laboratory Technical Report ARBRL-TR-02075, June 1978. AD #A058307
6.   L.H. Russell, "Simplified Analysis of the Bore Surface Heat Transfer Reduction in Gun Barrels as Achieved by Using Wear-Reducing Additives," Naval Surface Weapons Center Report TR-3378, October 1975.
7.   "Proceedings of the Tri-Service Gun Tube Wear and Erosion Symposium," edited by Jean-Paul Picard and Iqbal Ahmad, March 1977.

The work that will be described in this report was undertaken in order to develop data on the effects that the burning of various propellants in combination with wear reducing additives have on the surface layer compositions of a typical gun steel, AISI 4340. Central to this study was the realization that ion beam analysis methods could be used to determine the properties of bore surfaces that bear most strongly on erosion. The experiments were designed so that shot by shot trends and correlations could be observed in a small number of rounds. Correlating these trends to existing wear data on widely used propellant/additive systems, leads to predictions concerning new and novel systems on the basis of relatively small expenditures of time, effort and money. These experiments had to be carried out in the laboratory where the maximum number of parameters could be controlled.

2. EXPERIMENTAL PROCEDURE

2.1 Test Firing Program

In order to control the largest possible number of experimental parameters as well as to allow non-destructive analysis of the steel surfaces exposed to burning propellants, contoured nozzles of 4340 steel were used. The 4340 steel, hardened to 42 Rockwell, closely resembles the composition and hardness of typical gun tube steel. Twelve of these nozzles were exposed in a 37 mm gun whose barrel was cut off and which was modified to act as a blow-out chamber. A sketch of this 37 mm chamber is shown in Figure 1. The 1/16" thick mild steel discs were used to contain the burning propellant gases until the pressure became high enough to rupture the disc and send the hot gases streaming over the nozzle surface causing the erosion. Each of twelve nozzles was fired with a different combination of the propellants M2, M30 and M1 and the additives TiO_2 wax (XM1), Talc Wax (TW), Polyurethane Foam (PUF) and no additive (NA). The main criterion for choosing these propellants was the large range of their flame temperatures from 2417°K for M1, 3040°K for M30 to 3320°K for M2.

With two exceptions, four shots were fired through each nozzle. The propellant charge was chosen to give approximately the same pressure-time trace with each of the three propellants. The pressures were measured in the chamber with a Top-Hat strain gauge and the pressure-time trace was recorded for each shot on film. A sample pressure-time trace is shown in Figure 2. The M2 charge mass was taken directly from previous BRL work[8] and the others were matched to it by the pressure-time trace. The amount of the additives which were used was also taken directly from ref. 8. All the additives came in sheet form, were rolled around the forward part

8. Michael A. Schroeder and Masahiro Inatome, "The Relationship Between Chemical Composition and Wear-Reducing Effectiveness of Some Laminar Additives for Gun Propellants: Polyvinyltetrazole," Ballistic Research Laboratory Memorandum Report 2512, August 1975. AD #B007029L
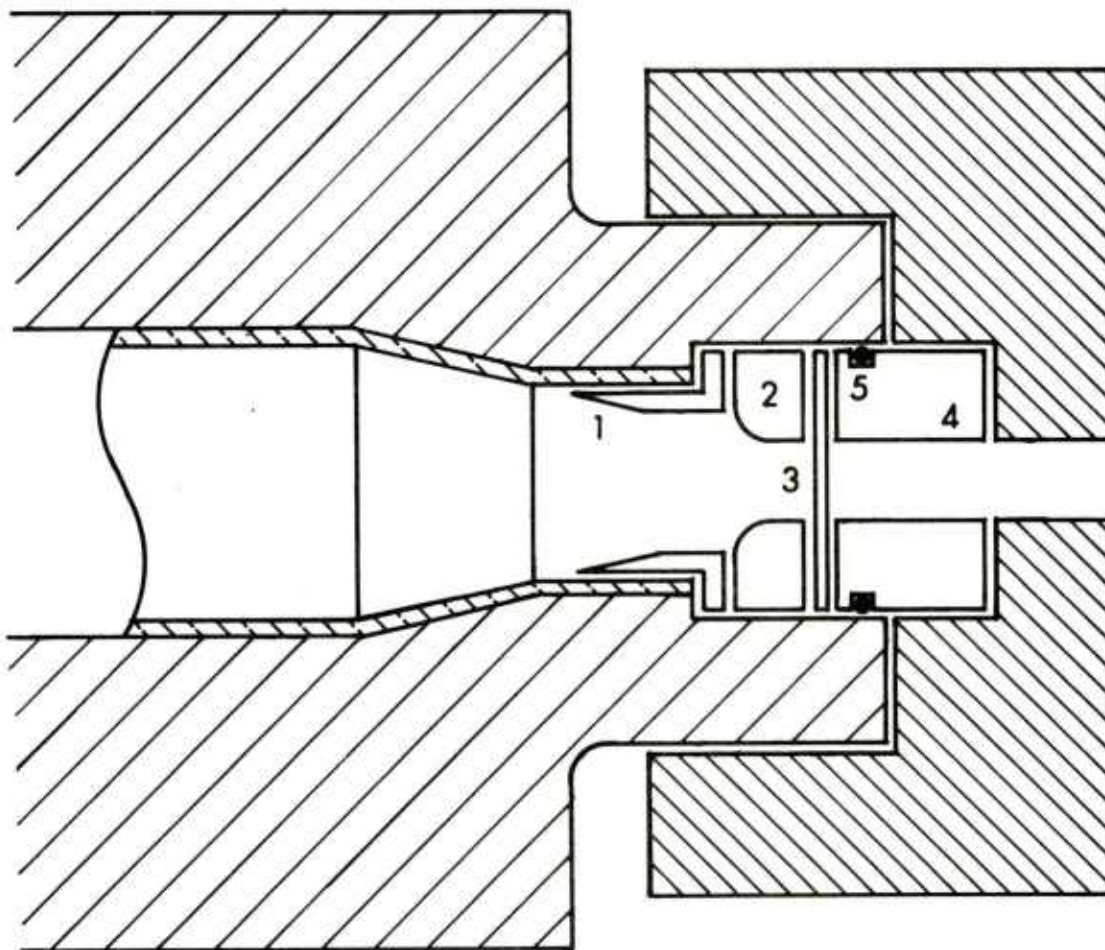
1. RETAINING RING
2. NOZZLE
3. BLOWOUT DISC
4. SPACER
5. O-RING SEAL

Figure 1.   37mm Vented Chamber.

35 MPa/cm

2 ms/cm

Figure 2. Pressure-time trace for nozzle #10.

of the propellant bed and the ends were flapped. This configuration of the additive sheet has been shown to be the most effective at erosion reduction[8,9]. The propellant/additive parameters under which all of the twelve nozzles were fired are shown in Table I. The additive masses shown are averages for all shots taken with the given configuration.

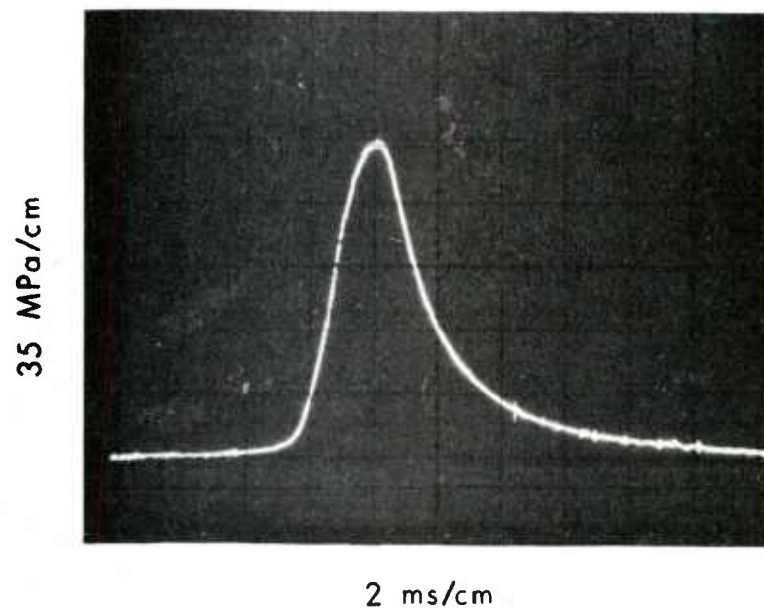After each shot, the nozzles were cleaned with a water-detergent wash, rinsed in alcohol and the mass losses measured. The record of the pressure and mass loss measurements is shown in Table II. The averages and their mean standard deviations are shown for the peak pressures, the durations of the pressure pulses and the mass losses for each of the propellant/additive combinations. The variation in the peak pressure was found to be up to 10% and is most likely due to the variation in the manner in which the steel blowout discs ruptured. The small, but clear, increase in the pressures when additives were used was probably due to the increase in the amount of gas from the burning additives as well as the lowering of the effective volume of the chamber. The duration of the propellant burn seems to be mainly a function of the propellant type. It is significant to the extent that a longer time at a temperature above surface melting point produces more erosion. However, since no attempt was made to measure the nozzle surface temperatures in this experiment, the pulse duration does not contribute significantly in our conclusions.

The shot-to-shot variation in the mass losses indicated by the standard deviations in Table II, was somewhat larger than the measurement uncertainties of ± 0.1 mg would allow. However, other experiments with this chamber as well as with other test fixtures[3] have shown very similar shot-to-shot variations. Although the reason for this variation is not known, we speculate that localized random variations in the flame patterns can be responsible. Another possibility is that the blow-out discs may have sheared unevenly, providing uneven regions of hot gas flow.

2.2 Ion Beam Analysis

After the cleaning and mass loss measurements, the nozzles were subjected to ion beam analysis. Most of the details of the technique are fully described in an earlier report[10] and so will not be discussed. However, since a different accelerator was used in these studies, operating at a different beam energy, there are some differences in details which will be pointed out when appropriate. It is recommended that in order to fully understand the IBA method, Ref. 10 and references therein should be studied.

9. Timothy L. Brosseau and J. Richard Ward, "Reduction of Heat Transfer in 105 mm Tank Gun by Wear-Reducing Additives," Ballistic Research Laboratory Memorandum Report, BRL-MR-2698, November 1976. AD #B015308L
10. A. Niiler, J.E. Youngblood, S.E. Caldwell and T.J. Rock, "An Accelerator Technique for the Study of Ballistic Surfaces," Ballistic Research Laboratory Report No. 1815, August 1975. AD #A016899

Table 1. Firing Data

Nozzle Numb./Add./ Rounds Fired	Propellant Type/Mass/Temp.	Peak Pressure (MPa)	Mass Loss (mg)
2/NA /4		165.5± 3.4	36.8±5.5
3/XM1/4	M2/85g	180.0±11.0	8.5±1.1
4/TW /4	3320°K	178.6±13.1	6.9±3.2
5/PUF/4		174.5± 3.4	9.9±5.0
6/NA /4		178.6± 5.5	13.0±1.0
7/XM1/4	M30/110g	186.2± 4.8	5.9±3.6
8/TW /5	3040°K	182.1±17.2	4.6±1.9
9/PUF/4		187.6± 4.8	6.5±2.5
10/NA /4		169.0± 3.4	4.9±1.9
11/XM1/3	M1/105g	179.3±15.2	4.0±1.1
12/TW /4	2417°K	180.0±14.5	3.9±1.2
13/PUF/4		179.3± 4.8	3.4±1.9

Table 2. Results of Pressure and Mass Loss Measurements

Nozzle	Propellant/ Additive	Peak Pressure (K psi)	Duration FWHM (msec)	Mass Loss (mg)
2	M2/NA	24.0±0.5	2.20±0.10	36.8±5.5
3	M2/XM1	26.1±1.6	2.08±0.16	8.5±1.1
4	M2/TW	25.9±1.9	2.06±0.16	6.9±3.2
5	M2/PUF	25.3±0.5	2.14±0.10	9.9±5.0
6	M30/NA	25.9±0.8	2.54±0.04	13.0±1.0
7	M30/XM1	27.0±0.7	2.48±0.04	5.9±3.6
8	M30/TW	26.4±2.5	2.68±0.24	4.6±1.9
9	M30/PUF	27.2±0.7	2.50±0.08	6.5±2.5
10	M1/NA	24.5±0.5	2.36±0.06	4.9±1.9
11	M1/XM1	26.0±2.2	2.26±0.14	4.0±1.1
12	M1/TW	26.1±2.1	2.28±0.12	3.9±1.2
13	M1/PUF	26.0±0.7	2.28±0.10	3.4±1.9

The IBA method is outlined as follows: A high velocity, focused beam of ions, deuterons in this case, is generated by an accelerator, and directed onto the surface of a sample to be analyzed. As the deuterons impinge on the sample, they can undergo nuclear reactions as well as elastic scattering with the nuclei of the sample's constituents. The type of particles that emerge from these encounters, as well as the energies of these particles, is very specific to the type of target nucleus with which the encounter takes place. In addition, the number of a given type of emitted particles as well as its observed energy distribution can be used to deduce concentrations and depth profiles of the nuclei in the surface with which the interactions took place. Figure 3 is used to illustrate this method. The insert in this figure shows a surface containing iron, carbon, nitrogen and oxygen. As the deuteron beam enters the surface, one of the many different types of encounters the deuteron particles undergo is elastic, billiard ball type, scattering from any of the constituents. If the scattered particles are detected at an angle greater than 90° with respect to the beam direction, this elastic interaction is known as Rutherford Backscattering (RBS). The spectrum shown in Figure 3 shows this RBS distribution to the left. Other types of encounters between the beam deuterons and target are exothermic nuclear reactions (NR) with the carbon, nitrogen and oxygen in the surface. In these reactions, higher energy protons and α-particles are emitted. The proton peaks due to C,N and O are also shown in figure 3 at the right. In Ref. 10, the NR analysis was done on α-particles emitted from oxygen.

Both the RBS distribution and the NR peaks can be used to obtain specific information about the surface layers. The NR peaks are very specific in identifying the constituents of the surface while the shape of the RBS distribution is very sensitive to the total amount of "contamination" on the surface. The most detailed information about concentrations and depth profiles of C,N and O is obtained from the NR peaks. The area under a given peak is related to the concentration of that element in the surface while the shape of a peak, especially its width, is related to the depth profile. In order to quantitatively determine these concentrations and depth profiles, a computer program which models the experimental spectrum by numerical integration, is used. This program will be described in a later section.

A deuteron beam of nominal energy of 0.665 MeV, obtained from the BRL Cockcroft-Walton accelerator was used for these analyses. The beam energy was checked periodically and referenced to the 0.669 MeV resonance in the $^{19}F(\rho,\alpha\gamma)^{16}O$ reaction. The uncertainty in the beam energy was found to be ± .003 MeV. Samples were mounted in a scattering chamber normally held at a pressure of 2×10^{-6} torr. A silicon surface barrier detector was used for the simultaneous detection of both the RBS and NR products. This type of detector produces an output current pulse which is proportional to the energy of the incident charged particle. These current pulses are passed through a charge sensitive preamplifier, a high resolution linear amplifier and finally stored in a multi-channel pulse height analyzer.
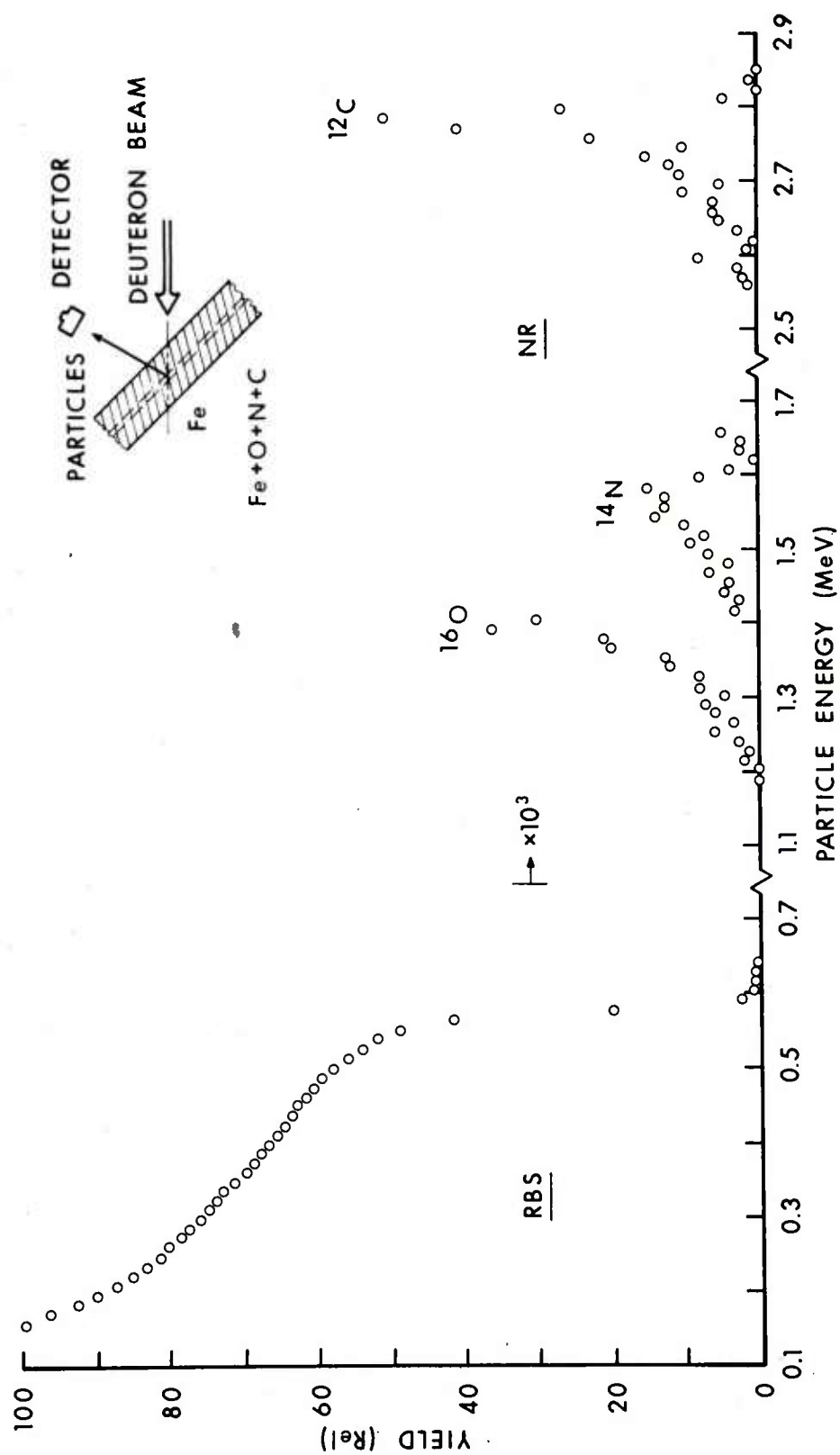
Figure 3. Ion Beam Analysis Schematic and Spectrum.

17

The RBS distribution and NR peaks shown in figure 3 result from this type
of signal analysis. In order to obtain the maximum detector resolution
of 0.012 MeV for 5.5 MeV alphas, a pulse pile-up rejection feature is
incorporated into the electronics. In a pulse counting experiment such as
this, it is possible for two independently generated particles to produce
overlapping pulses in the detector/preamplifier/amplifier/analyzer chain.
When such a double event occurs, the total system resolution is degraded
and under some conditions, the spectral shapes can also be distorted. The
pulse pile-up rejection circuitry used eliminated about 95% of these double
events as long as the two pulses were more than 75 nsec apart and produced
by particles with energies greater than 50 keV. The samples were enclosed
by an electron suppression shield permitting accurate beam charge measure-
ments. The beam current integrator used to measure beam flux was gated
to correct for the electronic system dead time.

3. ANALYSIS PROCEDURE

3.1 Program PROFILE

The program PROFILE was used to analyze the RBS distributions and
the NR peaks from the nozzles in order to obtain the concentrations
and depth profiles of the surface contaminants. A complete description
of the program as it was originally used is given in Ref. 10 but since
significant changes have been incorporated since then, a detailed
description will also be given now.   Additional information including
a listing and a cataloging of the description for its use on the BRL
CDC 7600 computer is given in reference 11.

The procedure used in the calculation is essentially an iterative
fitting of the experimentally measured spectrum. The sample surface is
divided into a number of layers (up to 100), each of which is assigned a
thickness and a specific composition which may include up to five types
of atoms. All of the experimental parameters such as beam energy and
intensity, detector geometry and angle are known, while the specific com-
positions of the layers are the only unknowns. These latter quantities
are varied in proceeding to an acceptable fit to the data. Although in
the final analysis the layer compositions are the basic unknowns in the
experiment, there are a number of prior clues which eliminate the need for
a blind search through the whole periodic table. First, there is some prior
knowledge of the surface. The 4340 steel is over 95% iron and contains up
to .4% carbon. The fact that the surface was exposed to propellants
would also indicate that the propellant constituents such as carbon,
nitrogen and oxygen as well as some additives such as sulfur and barium
from $BaSO_4$ might be expected. Second, the presence of certain peaks in

11. A. Niiler, R. Birkmire and J. Gerrits, "PROFILE: A General Code
     for Fitting Ion Beam Analysis Spectra," Ballistic Research Laboratory
     Technical Report ARBRL-TR-02233, April 1980. AD #A084984

the NR region are definitive signatures of the presence of lighter elements such as carbon, nitrogen and oxygen. Finally, if there is enough of a given light element on the surface, it will produce a peak on top of the RBS distribution from iron.

The calculation proceeds by using layer constituents which result from "educated" guessing and determining the specific energy loss tables as a function of the layer, type of beam ion and the ion energy. The reference data for energy losses are obtained from the tabulations of Anderson and Ziegler[12]. The accuracy of the reference energy losses is very important because as the ions (deuterons, protons, α-particles) pass through the layers, they lose energy. Their final detected energy distributions are very sensitively dependent on the values of the energy losses as obtained from the reference tables.

At this point, each of the defined layers of the surface is subdivided into slabs in order to improve the energy resolution of the calculation and, in turn, each slab is illuminated by the same unit flux of deuterons. The deuterons are then required to undergo a particular type of interaction, either RBS or NR, with one of the layer constituents. The deuteron energies vary from one layer and slab to the next depending on how much energy loss has taken place since the beam entered the surface. In this calculation, the RBS and NR interactions are run separately, but contributions from all target constituents are added for each type of interaction. The probability for a given type of interaction is determined from the cross sections for those reactions. In all cases, the RBS probabilities are calculated from the Rutherford elastic cross sections whose values are given by

$$\sigma(E,\theta) = 1.296 \left(\frac{Z_1 Z_2}{E}\right)^2 \left(\csc^4 \cdot \frac{\theta}{2} - 2 \cdot \frac{M_1}{M_2}\right)^2 \tag{1}$$

where E is the deuteron energy,

θ is the scattering angle,

Z_1 is the deuteron charge,

Z_2 is the target charge,

M_1 is the deuteron mass,

and M_2 is the target mass.

12. H.H. Anderson and J.F. Ziegler, Hydrogen Stopping Powers and Ranges in All Elements, Pergamon Press, New York, 1977.
13. N. Longequeque, H. Beaumevieille, E. Ligeon, J.P. Longequeque, and M. Sandon, "Etude des Reactions $^{16}O(d,\alpha_o)$, $^{16}O(d,\rho_o)$ et $^{16}O(d,\rho_1)$ de 300 keV a 1 MeV (Resultats Experimentaux), Le Journal de Physique, 26, 1965, 367.

The NR cross sections for oxygen, the $^{16}O(d,p_1)^{17}O$ values were taken from Longequeue et al.[13]. For the $^{12}C(d,p_0)^{13}C$ reaction, we used values from Huez et al.[14]. For the $^{14}N(d,p_5)^{15}N$, we used values measured on the BRL Cockcroft Walton accelerator and the University of Delaware 2.5 MeV Van de Graaff. A description of this measurement is given in Section 4. The actual values of these three cross sections which were used for the oxygen, nitrogen and carbon analyses are shown in figure 4. The subscript on the outgoing particles (p_0, p_1, p_5) refer to the excited unclear state of the residual nucleus in the reaction.

Once the deuterons have interacted with the target nuclei in a given slab, the outgoing particles (either deuterons in the case of RBS or protons in the case of NR) are followed back out of the target, again undergoing the proper energy losses. Energy broadenings due to beam energy resolution, energy loss straggling and detector resolution are incorporated in the calculation at the appropriate points. When a distribution from a given slab has been followed to its exit from the surface, it is weighted by the cross section for the appropriate target constituent at the proper energy in the slab as well as the concentration of that constituent in the slab. The final energy distribution is made up of a series of gaussians whose centroids are determined by energy losses, whose widths are determined by energy broadenings and whose weights are determined by the cross sections and layer concentrations. These calculated distributions are fit by varying a scale factor to the experimental spectra by least squares methods. The concentration profiles are then adjusted and the calculation rerun until a satisfactory fit is achieved. The primary criteria for acceptable fits are a general agreement between the calculated and experimental shapes along with the lowest possible chi squared for the full calculation. The chi-squared is given by

$$\chi^2 = \frac{1}{N-I} \sum_i^N [A \cdot Y_c(i) - Y_e(i)]^2 / Y_e(i) \qquad (2)$$

where N is the number of points fit, I is the number of degrees of freedom, Y_c is the calculated distribution, Y_e is the experimental distribution and A is the least squares proportionality constant between the two distributions. Typically, I is given by

$$I = N_\ell (N_c - 1) \qquad (3)$$

where N_ℓ is the number of layers and N_c is the number of constituents

14. M. Huez, L. Quaglia and G. Weber, "Fonction D'Excitation de la Reaction $^{12}C(d,p_0)^{13}C$ Entre 400 et 1350 keV - Distribution Angulaires," Nucl. Inst. and Meth., 105, 1972, 197.
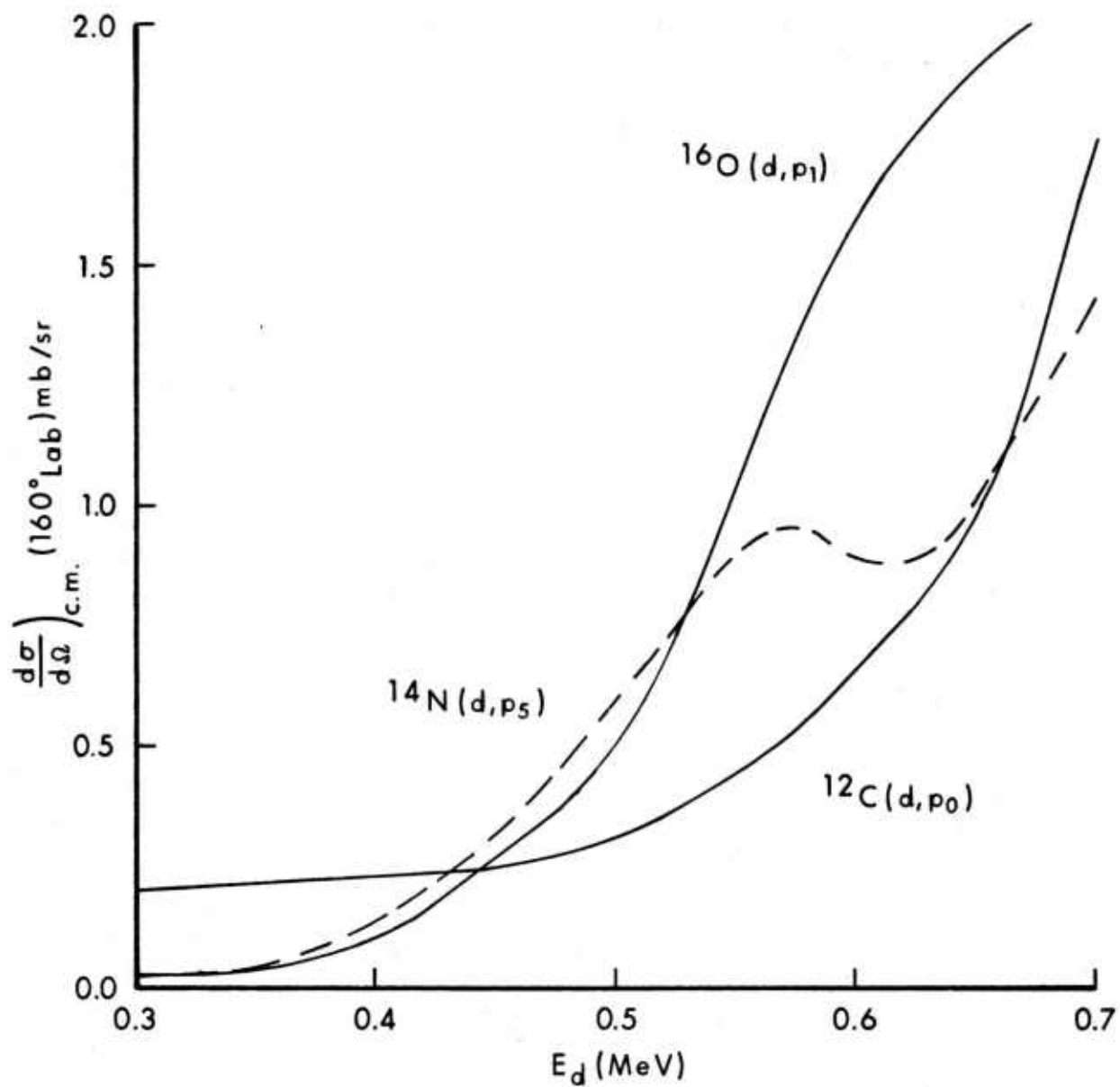
Figure 4.   (d,p) Cross Sections Used In Analysis.

per layer. Since usually it is possible to obtain acceptable fits within 5 to 10 iterations of the profiles by hand, no automatic search routines have been incorporated. Computer costs would be driven up considerably by such auto-fit routines.

The atomic concentrations of the various constituents of the surface are obtained in a straightforward manner from the profiles using the formula

$$N_i (at/cm^2) = \sum_j^{N_\ell} T_j A_o \frac{n_{ij}}{\sum_k^{N_c} n_{kj} A_k} \qquad (4)$$

where N_i is the atomic concentration for i^{th} constituent of the surface,

T_j's are the layer thicknesses,

A_o is Avogadros number,

n_{kj}'s are the atomic percentages of the kth constituent in the jth layer,

A_k is the atomic mass of the kth constituent and

N_ℓ and N_c are as previously defined.

The T_j's are program inputs whose values are chosen to yield the desired energy resolution for the calculation. Thus, the only input set which determines the final concentration values is the n_{kj}'s, the set of atomic percentages of the layers.

3.2 Discussion of Calculation

To understand the advantages and limitations of this calculational procedure in obtaining absolute concentrations and depth profiles, experiments done on a sample other than a nozzle will now be discussed. For this test case the sample is a polished flat slab of steel which was heated to produce an oxygenated surface layer. This sample was then analyzed by a .667 MeV deuteron beam resulting in RBS and NR spectra similar to those shown in figure 3. Using the PROFILE analysis described in the previous section, the concentrations for C,N,O, and Fe were determined and are shown in figure 5. The oxygen and carbon are surface peaked with both of them extending to the maximum probing depth of .55 mg/cm^2. There is very little nitrogen on this surface extending only to the .15 mg/cm^2 depth and the iron reaches its bulk value at the same .15 mg/cm^2 depth. The solid curve shown in figure 6 is the fit to the RBS and NR spectra obtained with the set of concentrations shown in figure 5. The chi-squared per point for this fit was 1.33.
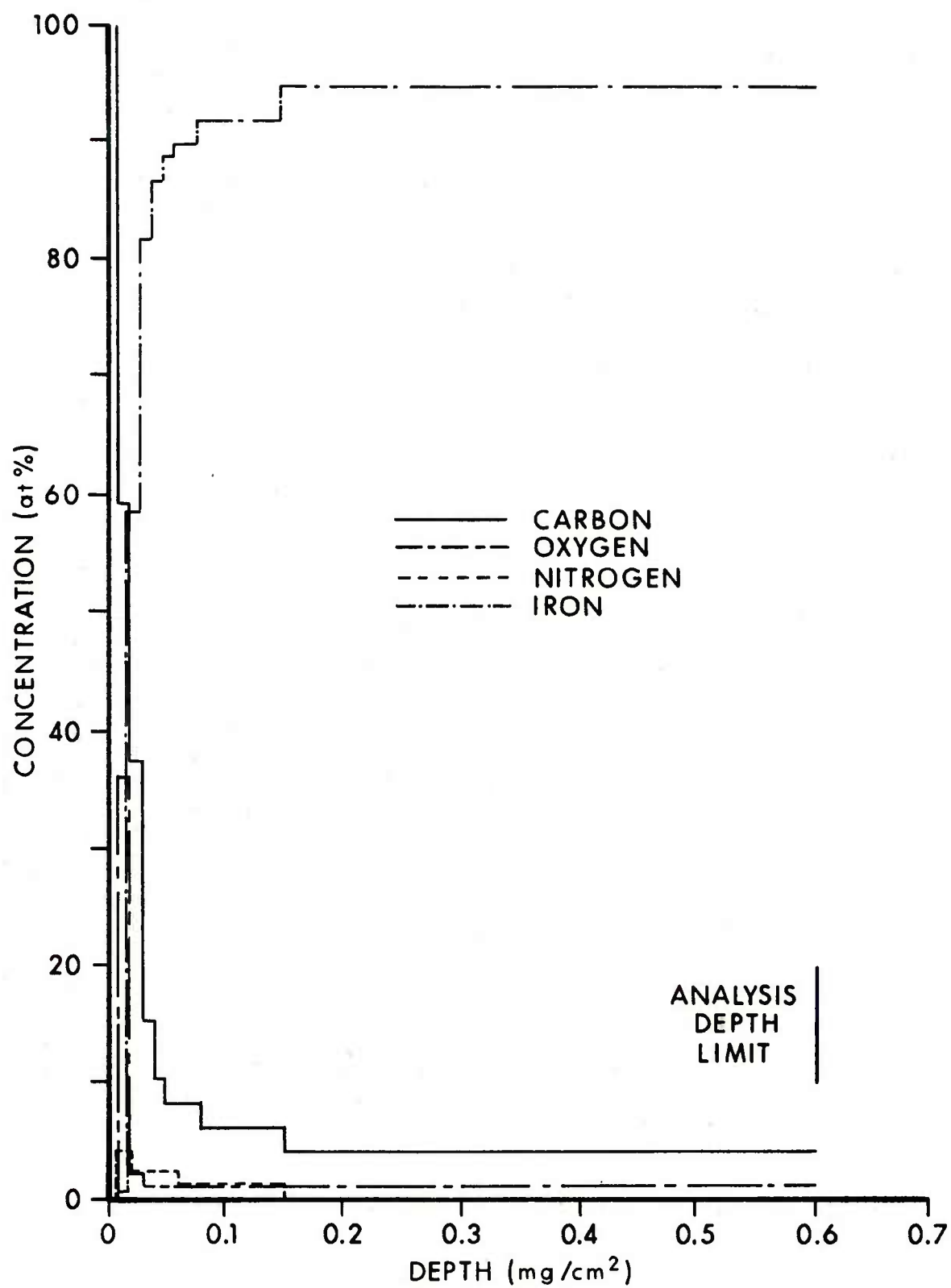
Figure 5. Concentration Profiles of O,N,C and Fe in Polished, Heated, Steel Slab.
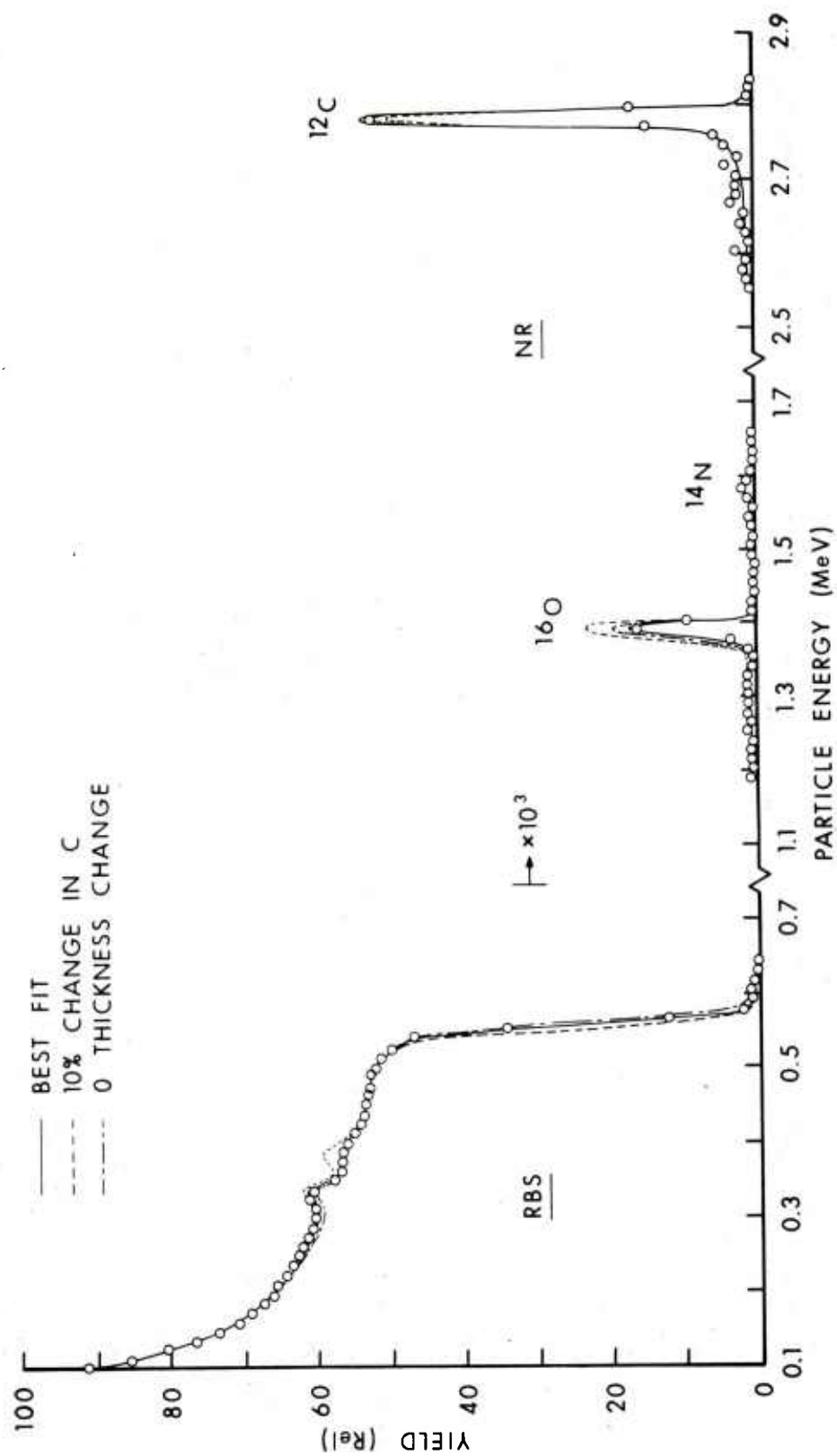
Figure 6. Fits to the RBS and NR distributions from the polished, heated steel slab obtained with various concentration profile sets. See text for explanation of the different curves.

To test the validity of IBA and the use of PROFILE, several checks have been performed on this sample. The sensitivity of the fit to variations in the profiles was examined. To determine the accuracy of this procedure for determining the concentration profile for a given constituent, the carbon concentrations were lowered by 10% over the full analyzed depth. The dashed curve in figure 6 shows the result of this calculation for which the chi squared was 4.21. The largest contribution to the increased chi square came from the fit to the RBS spectrum in the regions around .33 MeV and .56 MeV. There was almost no degradation in the fit to the carbon (d,p) peak in the NR region while the oxygen (d,p) peak was significantly affected. This illustrates that the profiles for all constituents must be correct in order for the overall fit to be good. It further demonstrates that the calculational accuracy in determining the concentrations is better than 10%. However, the calculated yields, and therefore the concentrations, are directly proportional to the specific Rutherford or Nuclear cross sections and, thus, are sensitive to the uncertainties of these cross sections. The Rutherford cross section values, as computed from equation 1, are within 2-10% of experimental values in this energy range while the measured NR values have at least a 10% absolute uncertainty. Consequently, the cross sections contribute a 10% absolute uncertainty to the concentrations. The total uncertainty on the concentration values is therefore somewhere between 10 and 15%.

A second variation in the profiles was examined to determine the depth resolution capabilities of this technique. The dot-dashed curve in figure 6 is the result of increasing the thickness of the oxygen layer from .01 to .02 mg/cm^2. The chi-squared for this fit was 5.94 with the poorer fit coming for the RBS distribution near .4 and .56 MeV and also in the region of the oxygen peak in the NR spectrum.

It has been shown[15] that surface roughness of the order of .02 to 1.0 microns will affect the RBS distributions if very small incident or exit angles are used. No effect was found for incident or exit angles above 5° or for scattering angles much larger than 100°. As in all of our experimental spectra the scattering angle is always 160° and the incident and exit angles are always greater than 20°, no effects due to surface roughness should be observable in our spectra. To illustrate this fact, we produced several surfaces with different roughnesses and ran the RBS and NR spectra through the standard analysis. As we reported in reference 16, the RBS distributions were consistent with assuming flat iron surfaces with small amounts of carbon in the outer layers. Based on these considerations, we neglect surface roughness effects totally in our calculations.

15. R.D. Edge and U. Bill, "Surface Topology Using Rutherford Backscattering," Nucl. Inst. & Meth., 168, 1980.
16. Andrus Niiler and Robert Birkmire, "Measurement of Oxygen and Nitrogen Profiles in Steel," Nucl. Inst. & Meth., 149, 1978, 301.

There is a maximum depth from which information about the various elemental concentrations can be obtained. This depth, referred to as analysis depth limit in subsequent discussion, depends on two major factors; the deuteron beam energy and the existence of interfering structures in the RBS or NR spectra. The beam energy dependence arises because the particles lose energy continuously in the surface layers, and thus a depth exists which is large enough so that particles with a given scattered energy cannot emerge, or emerge with energies too low to be detected. In figure 3, the energy cutoff of 0.15 MeV in the RBS spectrum is due to the electronic system threshold. Deuterons detected at this threshold energy were scattered from a depth of 0.55 mg/cm^2 with scattering from deeper layers yielding undetected, lower energy deuterons. The fact that interfering structures can affect the analysis depth is illustrated by the way the nitrogen peak of figure 3 runs into the oxygen peak. The lowest energy at which the nitrogen does not interfere with the oxygen is about 1.41 MeV. The protons which emerge from the sample with this energy were produced at a depth of about 0.53 mg/cm^2.

4. THE $^{14}N(d,p_5)^{15}N$ CROSS SECTION MEASUREMENT

The most commonly used reaction for nitrogen analysis is the $^{14}N(d,\alpha_1)^{12}C$.[17] However, the $^{14}N(d,p_5)^{15}N$ reaction cross section is about four times higher than the (d,α_1) and since the reaction gives the highest sensitivity for nitrogen detection, it has been used in this experiment. Although the (d,p_5) cross section has been determined at energies above 0.6 MeV[18], the data is sparse below that energy[19] and not adequate for ion beam analysis. In this section, the measurement of the (d,p_5) excitation function between 0.32 and 1.45 MeV deuteron energy and scattering angle of 160° in the laboratory will be described. The work in this section has been published in reference 20.

Two accelerators were used to collect the data in this experiment. The energy region from 0.40 to 1.45 MeV was covered in 0.05 MeV steps

17. J.W. Mayer and E. Rimini, Ion Beam Handbook for Material Analysis, Academic Press, New York, 1977.
18. G. Amsel, and D. David, "Microanalysis of Nitrogen by Means of the Direct Observation of Nuclear Reactions Applications," Rev. Phys. Appl. 4, 1969, 383.
19. A Valek, T. Vertse, B. Schlenk and I. Hunyadi, "A Study of the $^{14}N(d,p)^{15}N$ Reaction at Low Bombarding Energies," Nucl. Phys., A270, 1976, 200.
20. A. Niiler and R. Birkmire, "The $^{14}N(d,p_5)^{15}N$ Cross Section, 0.32-1.45 MeV," Nucl. Inst. & Meth. 168, 1980, 105.

at the University of Delaware 2 MeV Van de Graaff accelerator. The .872 MeV resonance in the $^{19}F(p,\alpha\gamma)$ reaction was used to calibrate the analyzer magnet. Beam slits after the analyzing magnet were set so as to give a beam with energy with accuracy better than ± .002 MeV throughout the entire operating range. The BRL Cockcroft-Walton accelerator was used to cover the energy range 0.32 to 0.70 MeV in energy increments of 0.005 MeV. The .340 and .669 MeV resonances in the $^{19}F(p,\alpha\gamma)$ reaction were used to calibrate the analyzer magnet on this machine. The .006 MeV width of the .669 MeV resonance and long term drifts in the system limited the Cockcroft-Walton energy accuracy to no better than ± .005 MeV.

Typically, 100 to 200 nA of deuterons were used during the measurements. Targets were self supporting foils made of a layered structure of copper, melamine and copper, all evaporated onto a 20 µg/cm^2 carbon foil. The total target thickness was estimated to be less than 150 µg/cm^2. Although this target structure gave the best stability under beam heating of all targets tested, the targets did degrade during the experiment. Later discussion will show that absolute target stability was not necessary. Spectra were taken only at 160° in the laboratory. At this angle, it was possible to arrange the beam-target-detector geometry in such a way that the incident and outgoing particles passed through only one 30-40 µg/cm^2 copper layer on their way to and from the melamine. The incident deuteron energy losses in the copper layer were at most .01 MeV and all reported bombarding energies have this correction factor applied. In addition, the melamine layers were thin enough so that neighboring (d,p) peaks from nitrogen, oxygen and carbon did not interfere with the analysis.

A sample of the spectra taken with a high resolution (12 keV for 5.5 MeV alphas) Silicon Surface Barrier detector is shown in Figure 7. Fast pulse pile-up rejection, 75 nsec resolving time, was used in order to keep pile-up signals from copper from producing additional backgrounds under the (d,p_5) peak.

Since the targets did not remain stable under beam heating, absolute cross sections for the $^{14}N(d,p_5)$ reaction could be obtained only by comparison to another ^{14}N cross section. The unresolved $^{14}(Nd,p_{1+2})$ peak was used. The (d,p_5) cross section is given by

$$\sigma_{(d,p_5)} = \sigma_{(d,p_{1+2})} \, Y_5/Y_{1+2} \tag{5}$$

where the σ's are the differential, laboratory cross sections and the Y's are the yields of the p_5 and p_{1+2} groups. In addition, neither the solid angle or beam charge measurements are needed to determine the cross sections by this method.
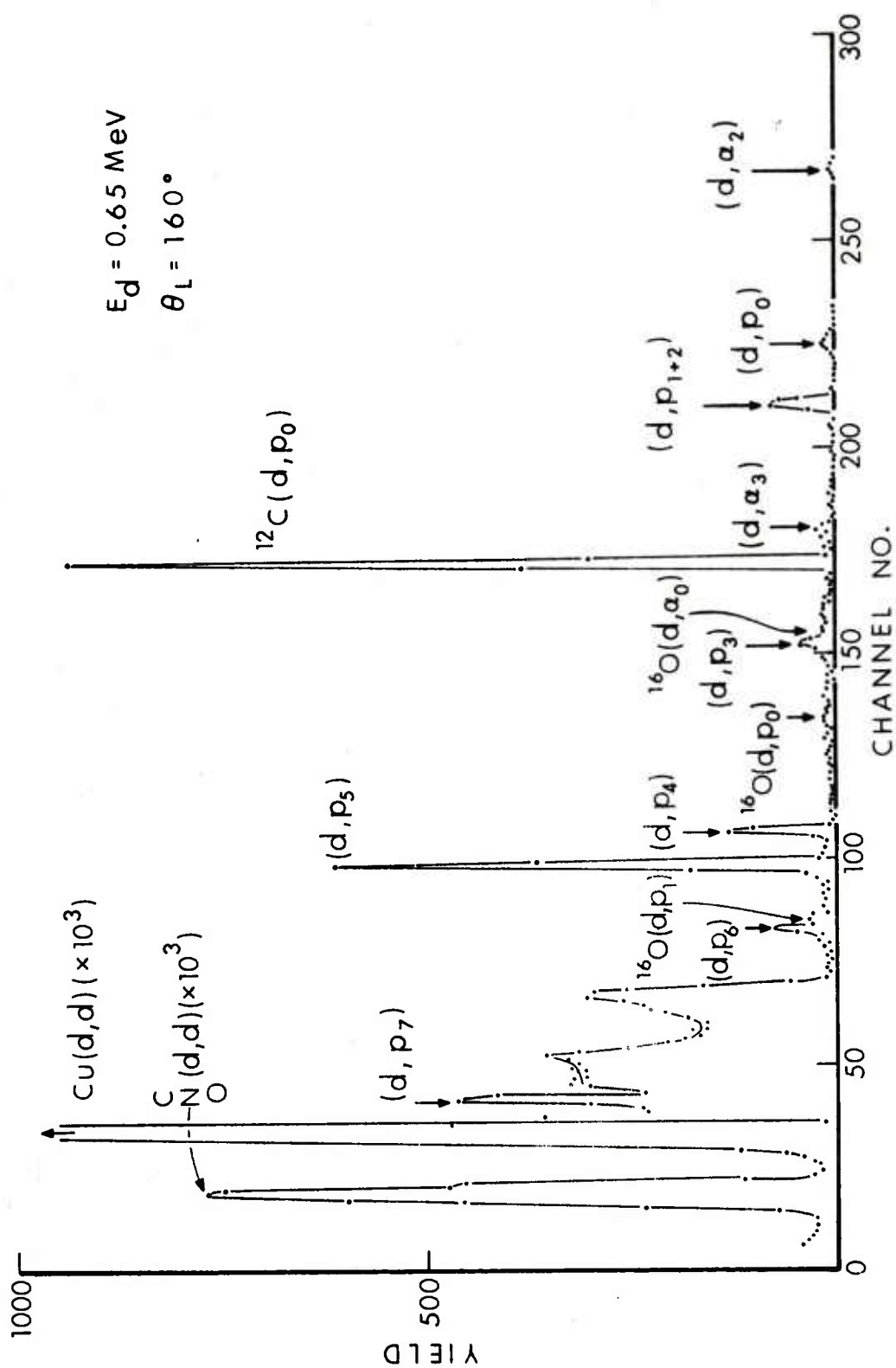
Figure 7. Spectrum of particles produced by 0.65 MeV deuterons at 160° from the Cu-Melamine-Cu-C Target.

28

Values for the reference $\sigma_{(d,p_{1+2})}$ cross section were obtained

from a smooth curve drawn through the available data of Amsel[18], Booth[21], and Valek[19]. Valek's data was followed below .6 MeV and Booth's and Amsel's data was used above .6 MeV. Although Porto[22] has performed measurements at energies above 1 MeV, it could not be read from the graph with enough accuracy for present purposes and was thus not used. Including the quoted 8% uncertainty, this type of interpolation procedure increases the final uncertainty on the reference cross-sections to about 10%. Over most of the energy range, this 10% is the predominant error in the measured values. However, at the lower energies, the counting statistics become more important so that the worst case uncertainty on the cross sections is about 35%.

The results of this experiment are shown in Figure 8 along with data from Amsel, Valek, and Porto. The Van de Graaff points are, in general, from a single data run. However, since the Cockcroft-Walton energy uncertainty was about .005 MeV, the data points are averaged over each .01 MeV energy interval. It can be seen that the present data generally agree within the uncertainty limits with the published data of Valek and Amsel. The fact that the agreement with Porto's data and Valek's point at .626 MeV is not as good can be attributed to the (d,p_{1+2}) normalization data that we used. The fact that all the data

shown are not at 160° is not significant since the angular distributions from Porto at 1 MeV and up seem to be quite flat at these backward angles. The small amount of structure indicated by the present data near 0.6 MeV has not been observed previously although Amsel's data does flatten out just before reaching .6 MeV. These new data improve the definition of the shape of the (d,p_5) cross section below 0.7 MeV.

5. RESULTS AND DISCUSSION

5.1 Concentrations

Following the procedures outlined in Section 3.1, concentration profiles were obtained for twelve nozzles. The concentrations which gave the best fits to the experimental spectra are shown in figures 9(a) through 20(a) while the fits are shown in figures 9(b) through 20(b). A glance at figures 9(b) - 20(b) can be used to obtain qualitative information about the amounts of C,N and O on the samples. The wider peaks indicate greater depths of penetration as can be seen by comparing figures 9(b) (Noz 2) and 17(b) (Noz 10), and the higher yields

21. D.L. Booth, F.V. Price, D. Roaf and G.L. Salmon, "The Differential Cross Sections for the Reactions $^{14}N(d,p)^{15}N$ and $^{14}N(d,\alpha)^{12}C$ Between 600 and 1000 keV," Proc. Phys. Soc. 71, 1959, 325.

22. V. Gomes Porto, N. Ueta, R.A. Douglas and O. Sala, "Deuteron Induced Reactions on ^{14}N," Nucl. Phys. A136, 1969, 385.
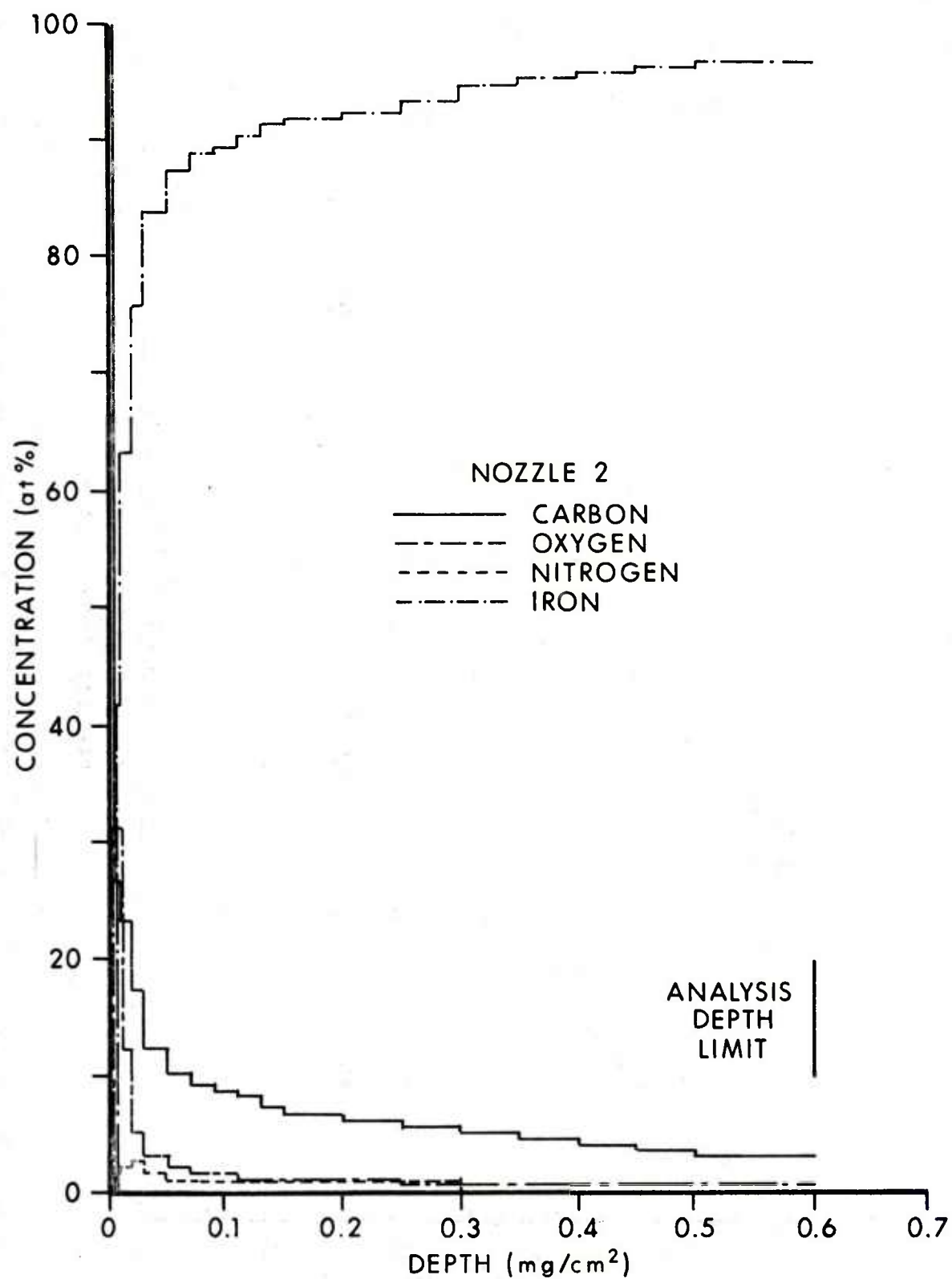
Figure 8. The laboratory cross section at 160° for the $^{14}N(d,p_5)^{15}N$ reaction. The line indicates the best estimate of the correct cross section and shows the values used in the analysis. The error bars indicate both counting statistics and systematic uncertainty from the reference cross sections. Error bars were omitted from some points for clarity but their size can be gauged from other points near-by.

30

Figure 9a.   Concentration depth profiles for nozzle #2.
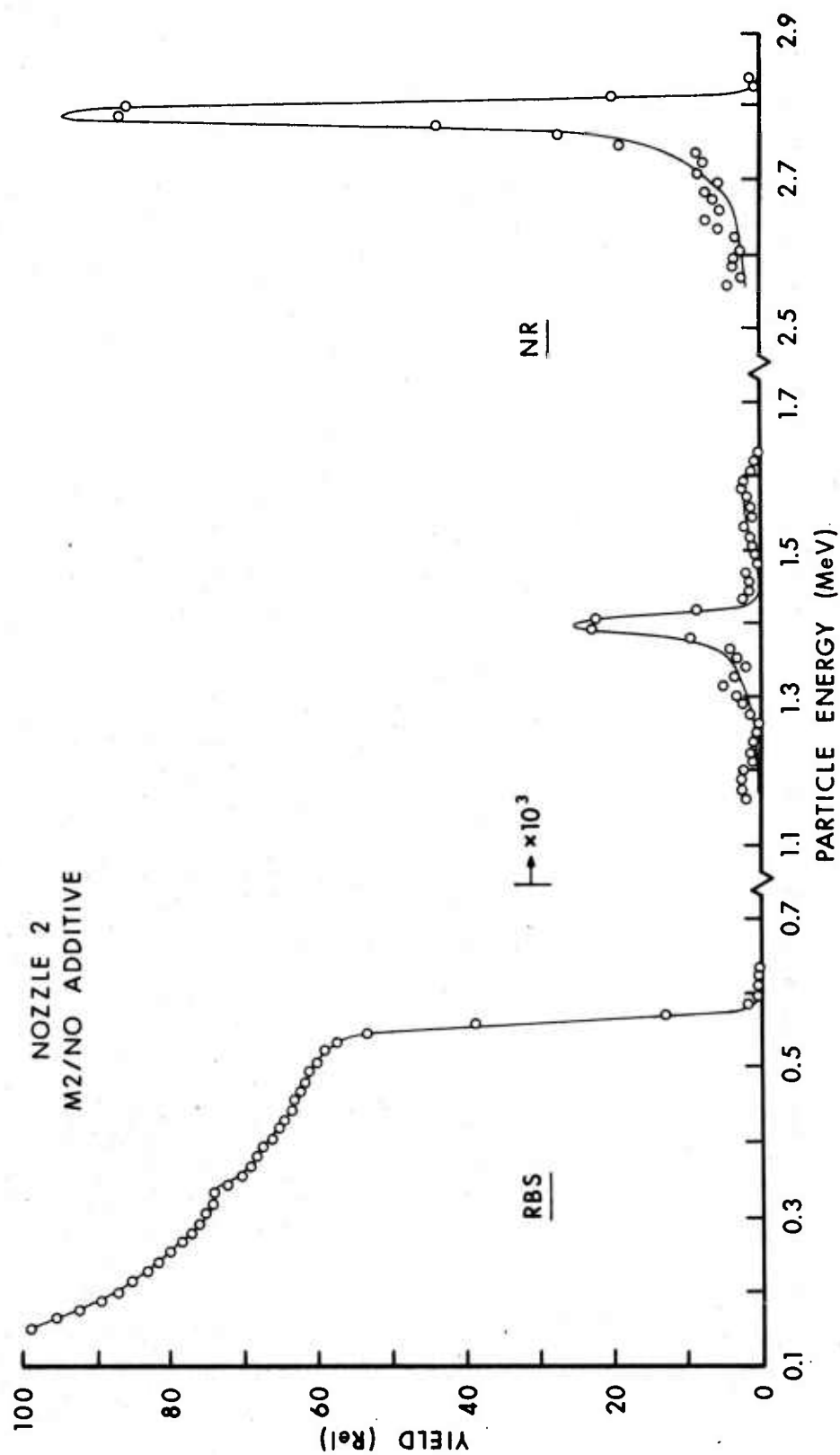
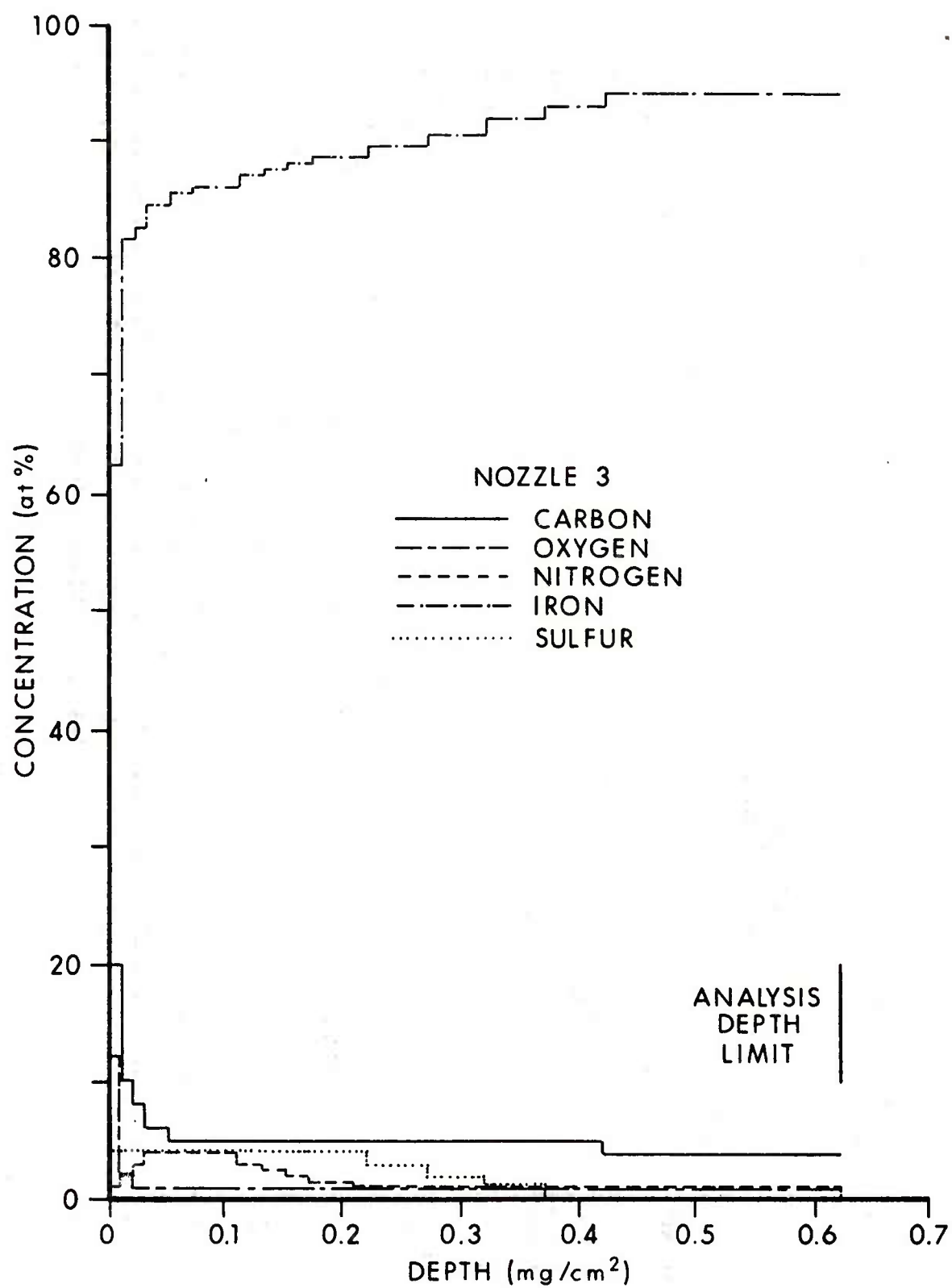Figure 9b. Fit to the RBS and NR spectra from nozzle #2 with concentration profiles shown in figure 9(a).

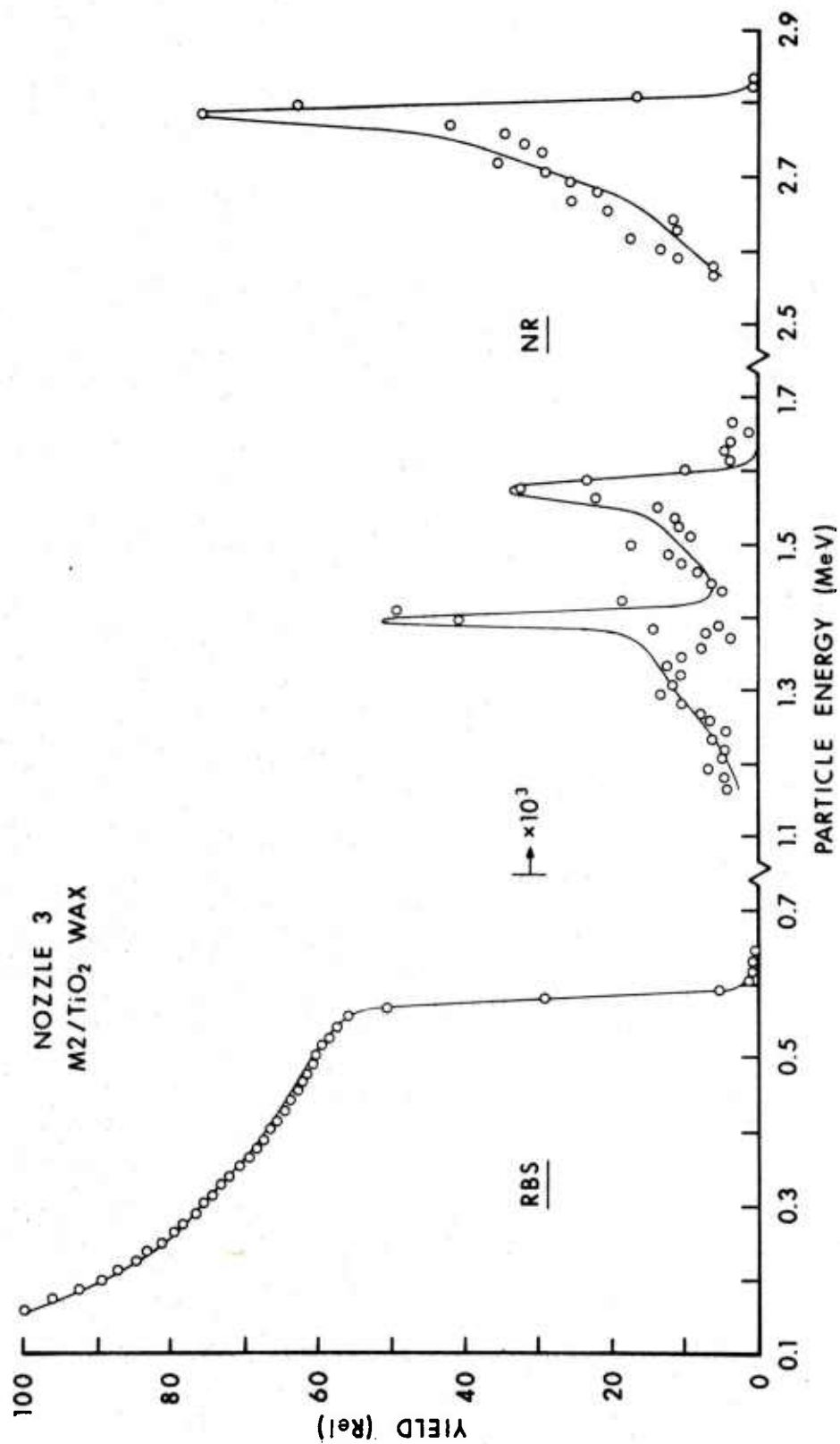Figure 10a.   Concentration depth profiles for nozzle #3.

Figure 10b. Fit to the RBS and NR spectra from nozzle #3 with concentration profiles shown in figure 10(a).
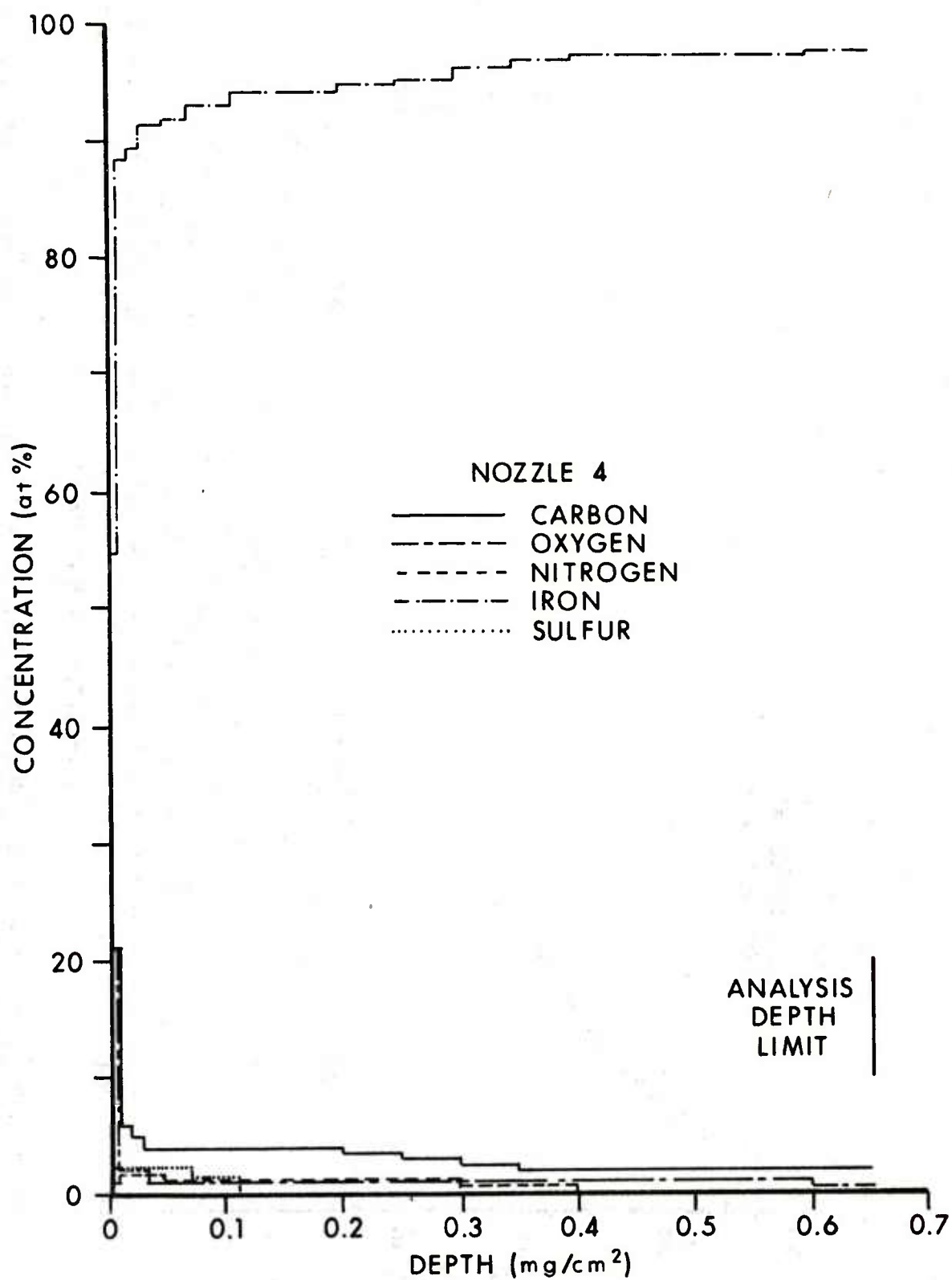
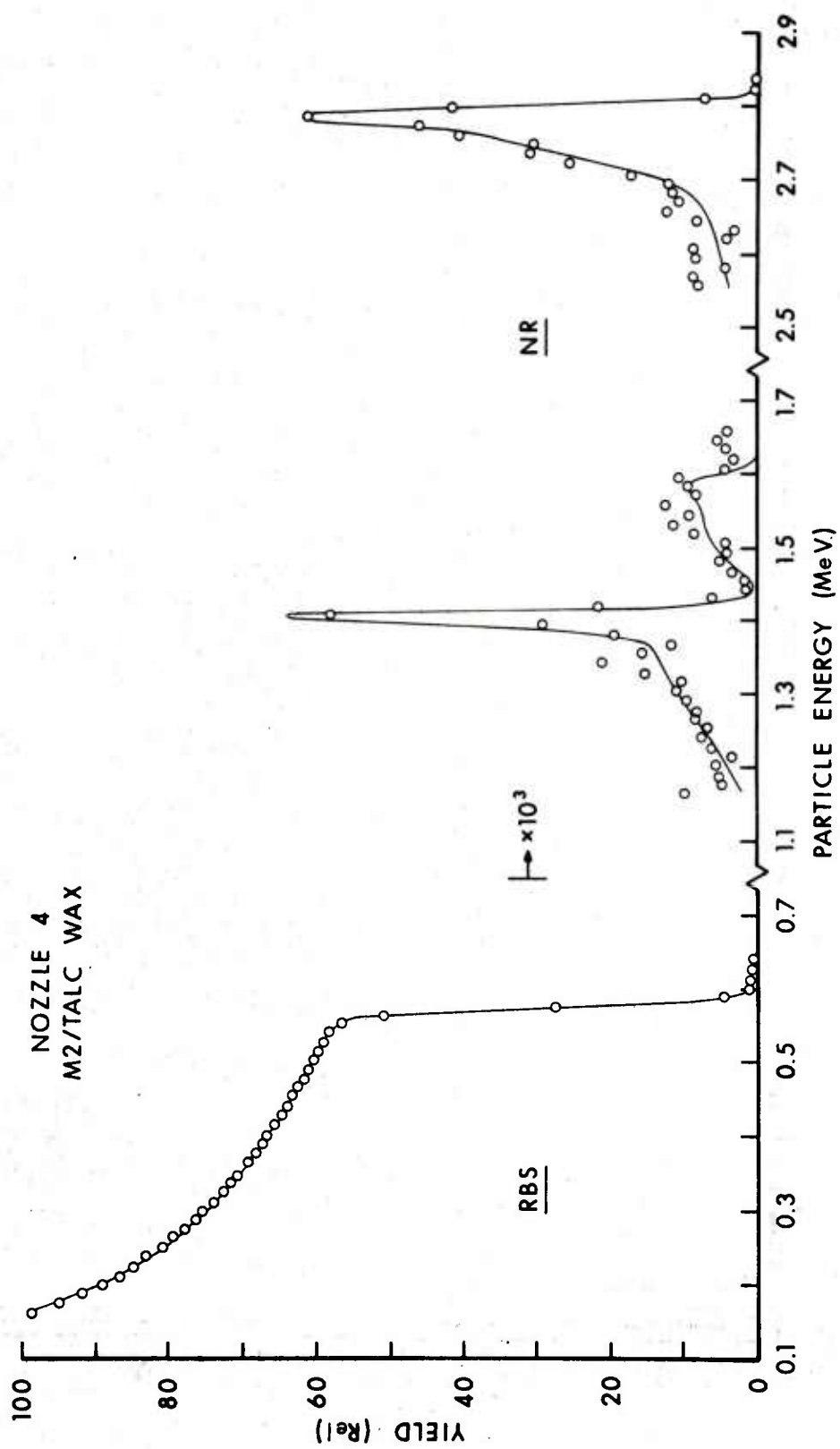Figure 11a.   Concentration depth profiles for nozzle #4.

Figure 11b. Fit to the RBS and NR spectra from nozzle #4 with concentration profiles shown in figure 11(a).

Figure 12a.   Concentration depth profiles for nozzle #5.

Figure 12b. Fit to the RBS and NR Spectra from nozzle #5 with concentration profiles shown in figure 12(a).

38

Figure 13a. Concentration depth profiles for nozzle #6.

Figure 13b. Fit to the RBS and NR spectra from nozzle #6 with concentration profiles shown in figure 13(a).
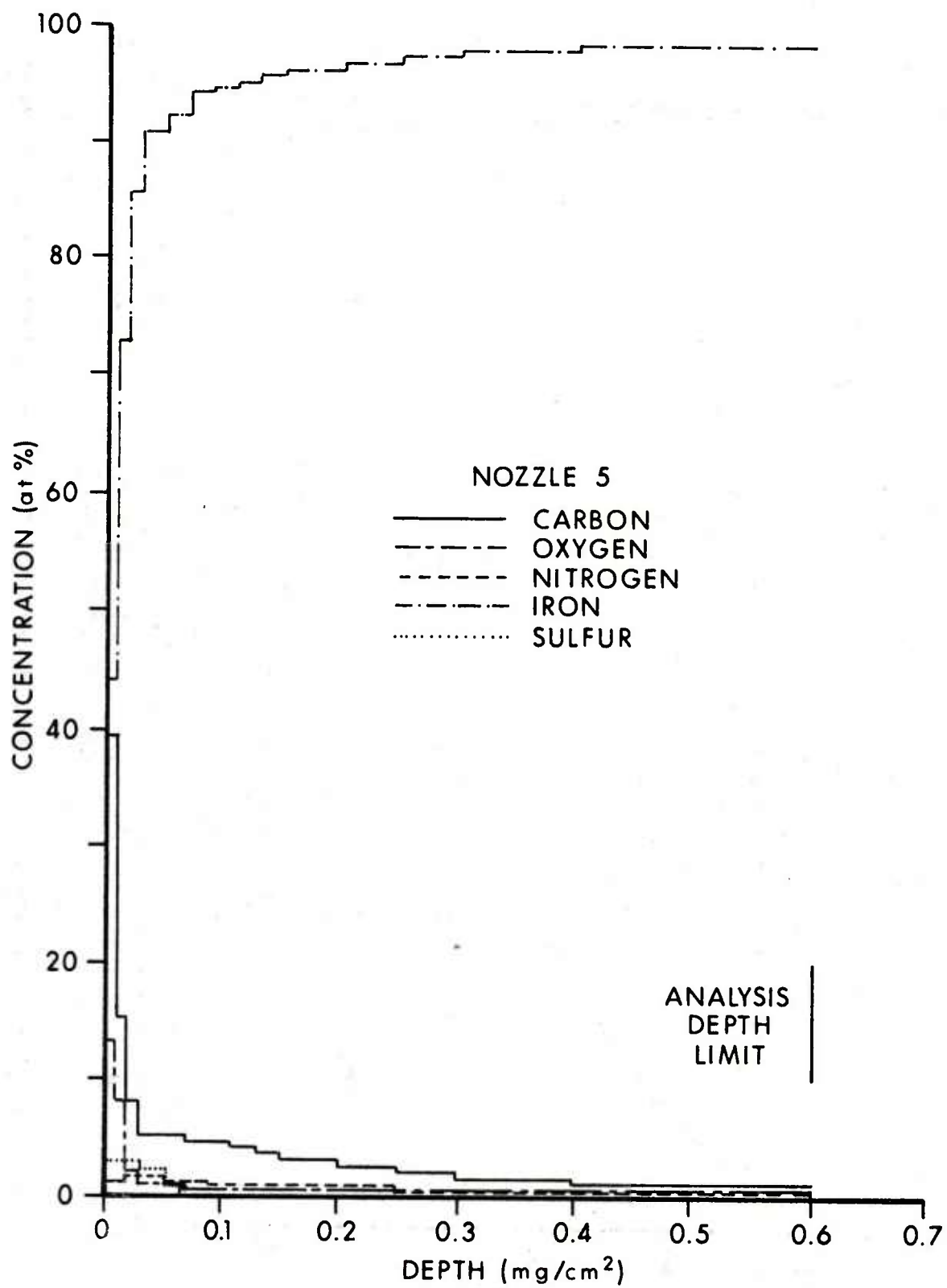
Figure 14a. Concentration depth profiles for nozzle 7.

Figure 14b. Fit to the RBS and NR spectra from nozzle #7 with concentration profiles shown in figure 14(a).

42

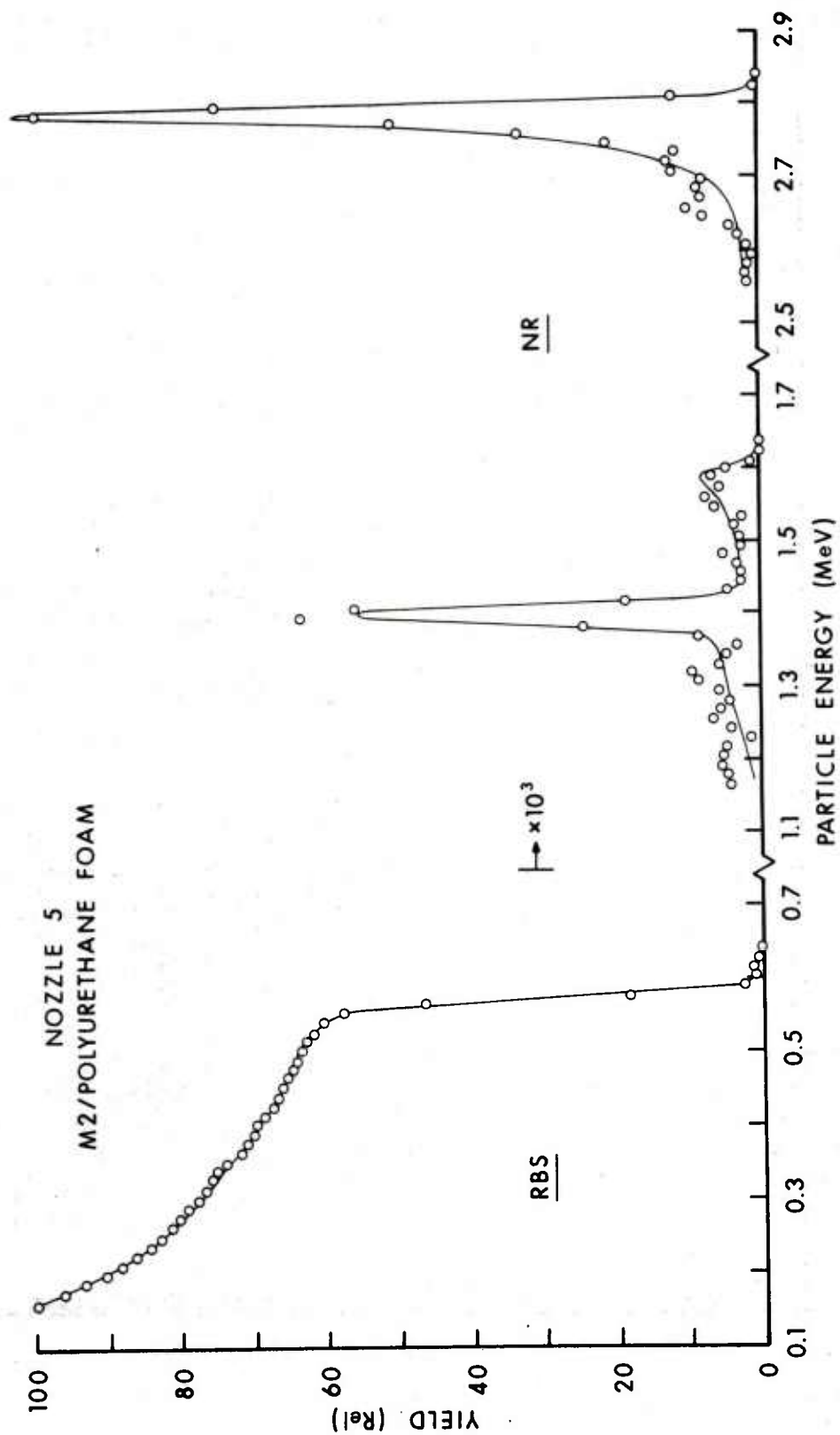Figure 15a. Concentration depth profiles for nozzle 8.

Figure 15b. Fit to the RBS and NR spectra from nozzle #8 with concentration profiles shown in figure 15(a).
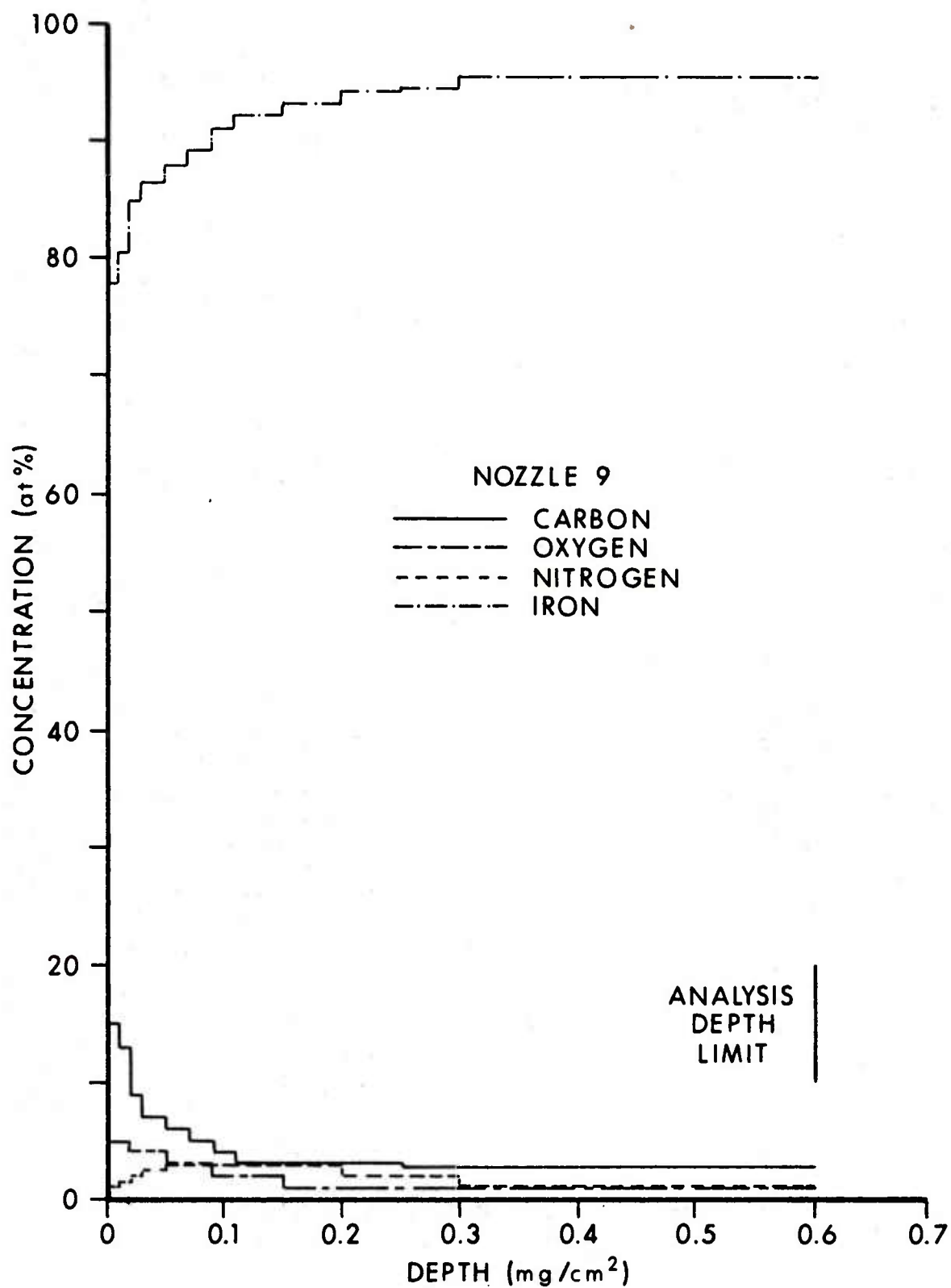
Figure 16a.   Concentration depth profiles for nozzle #9.
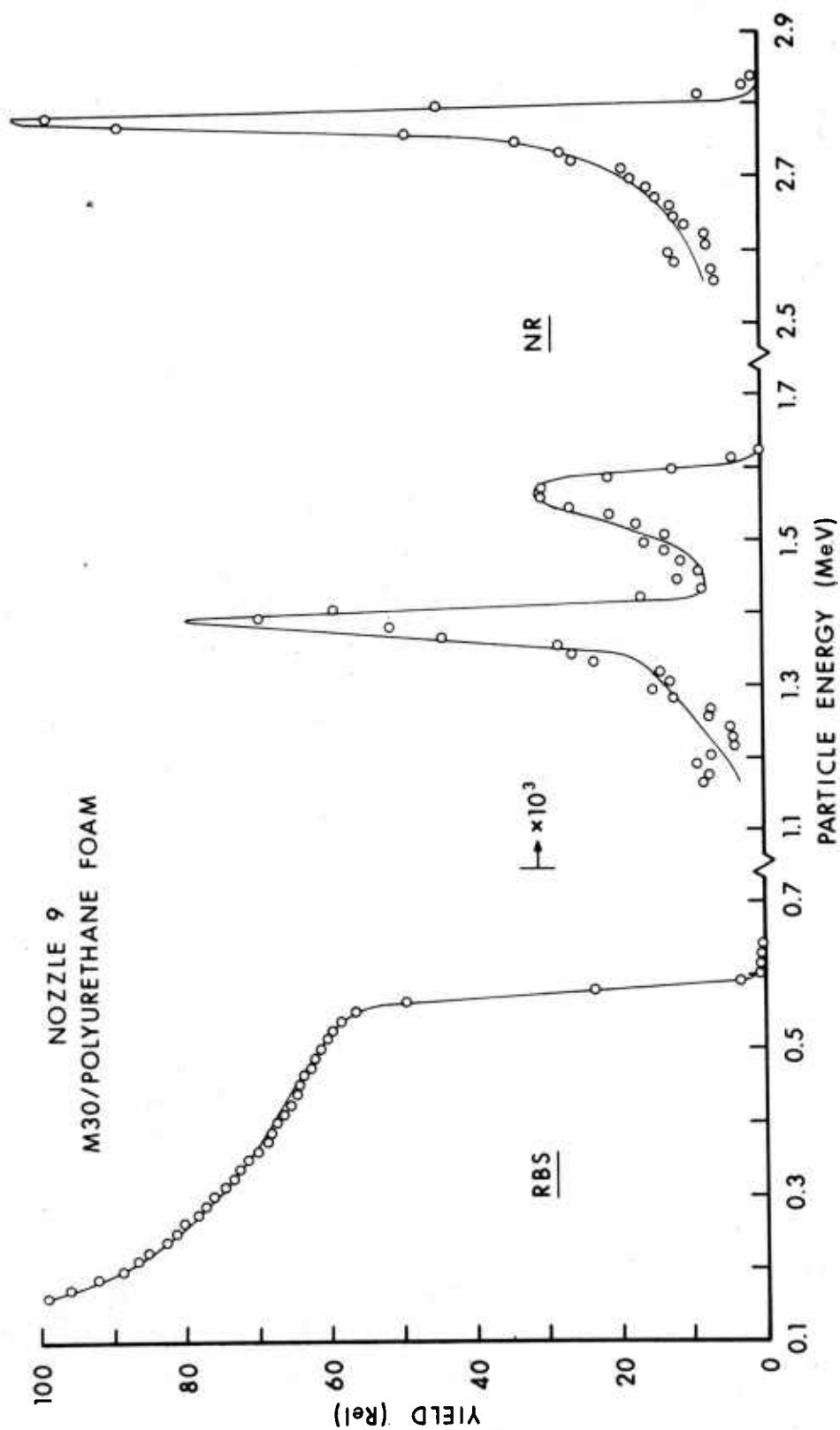
Figure 16b. Fit to the RBS and NR spectra from nozzle #9 with concentration profiles shown in figure 16(a).
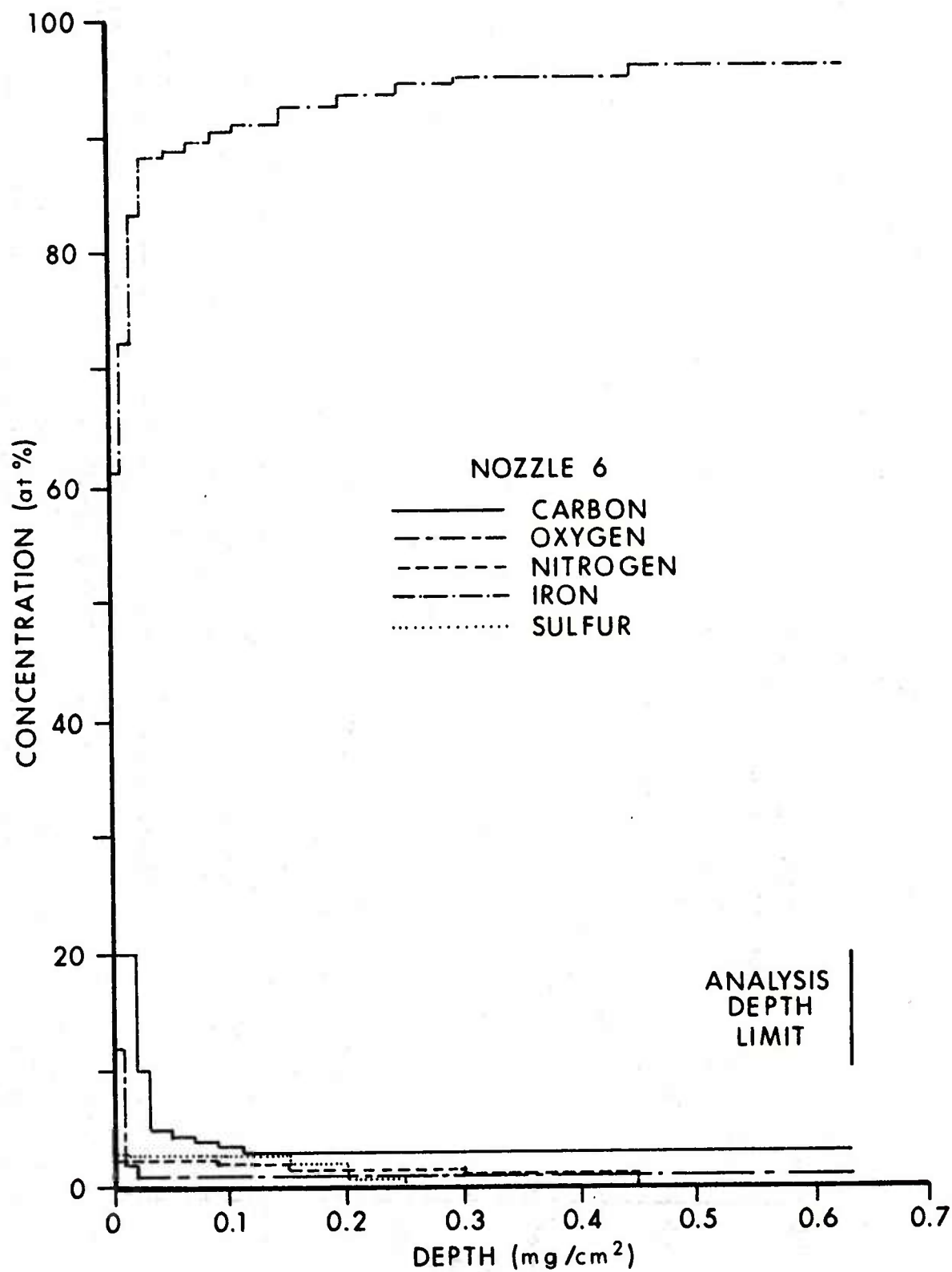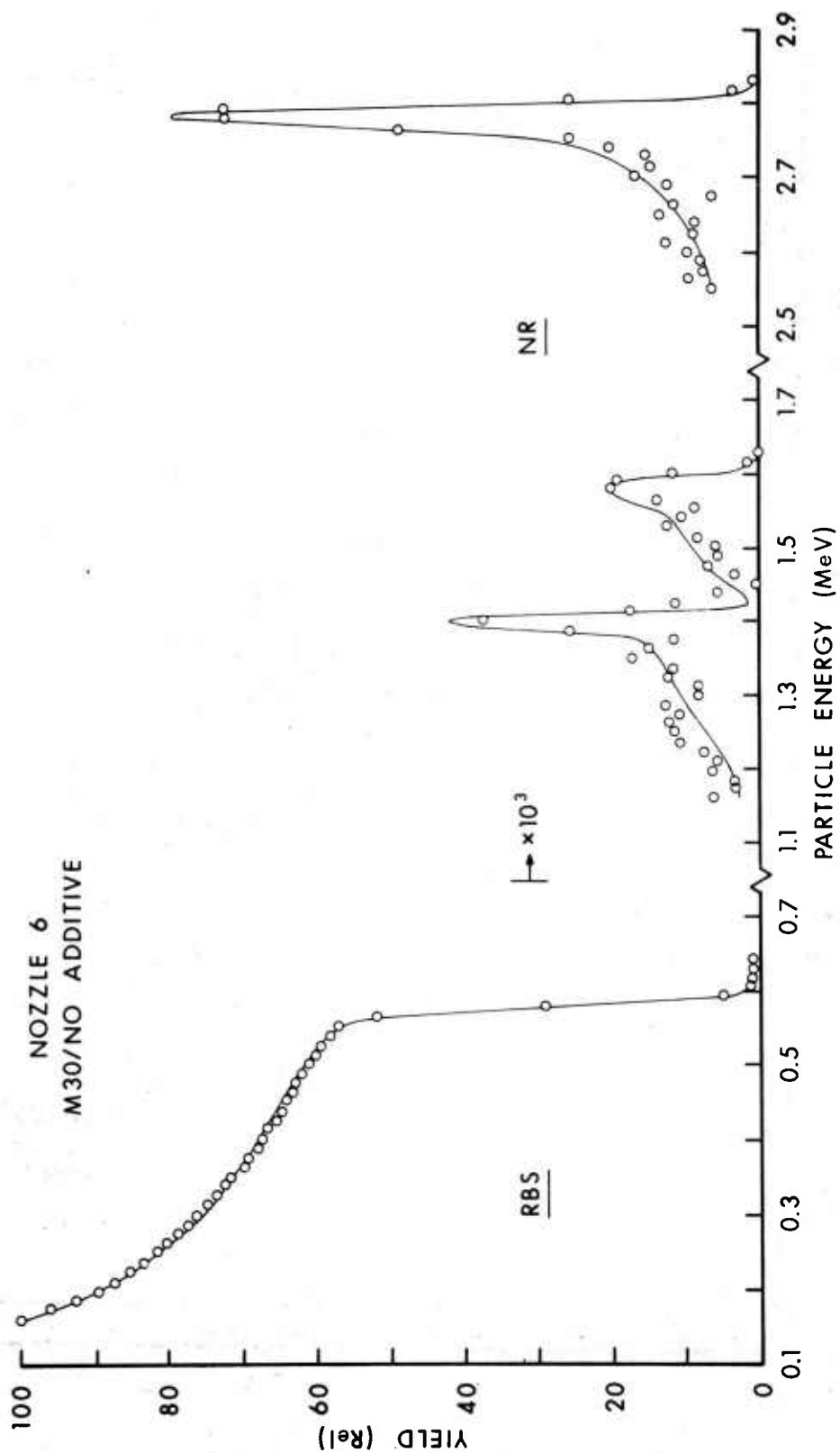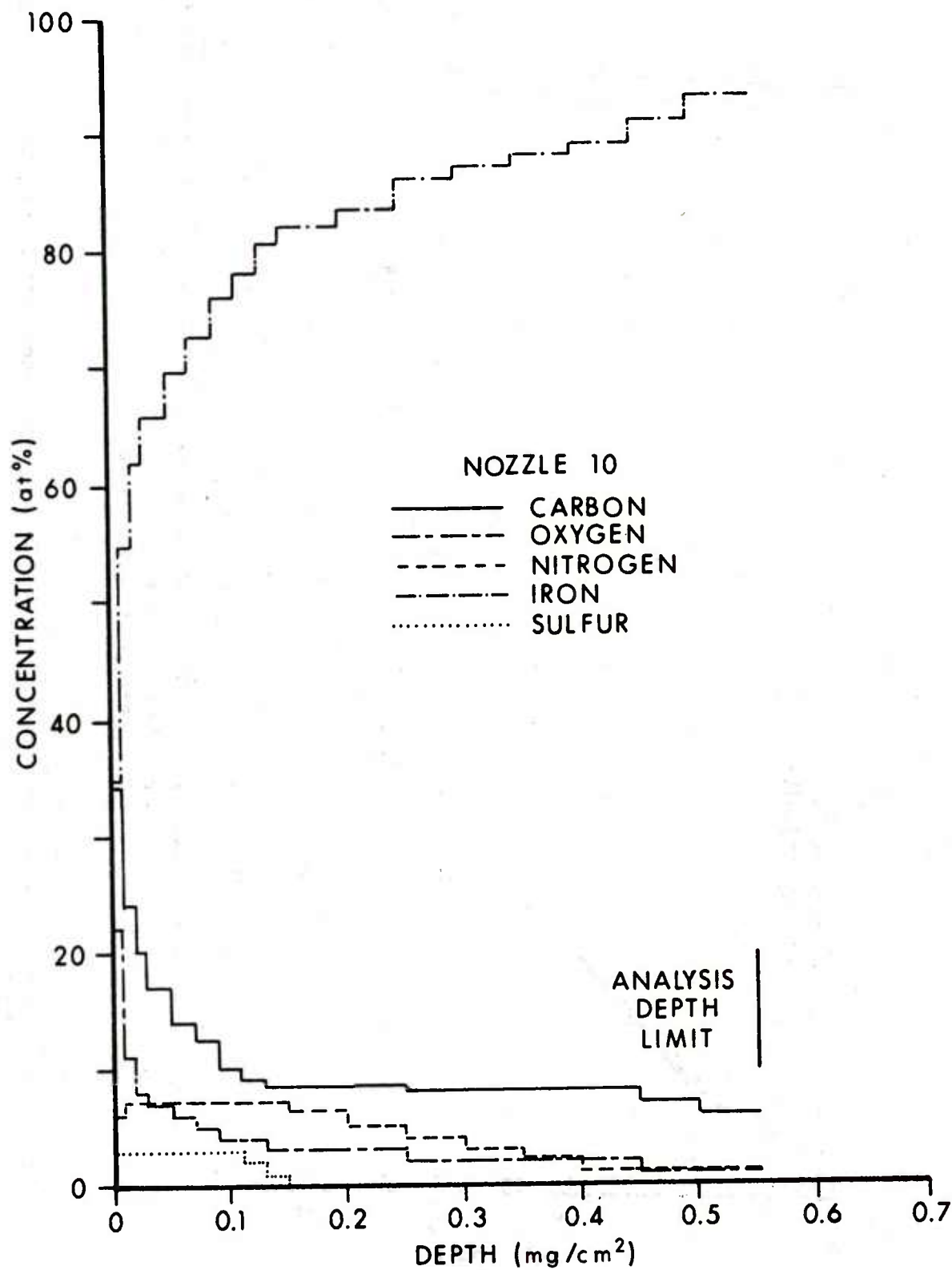
Figure 17a.   Concentration depth profiles for nozzle #10.
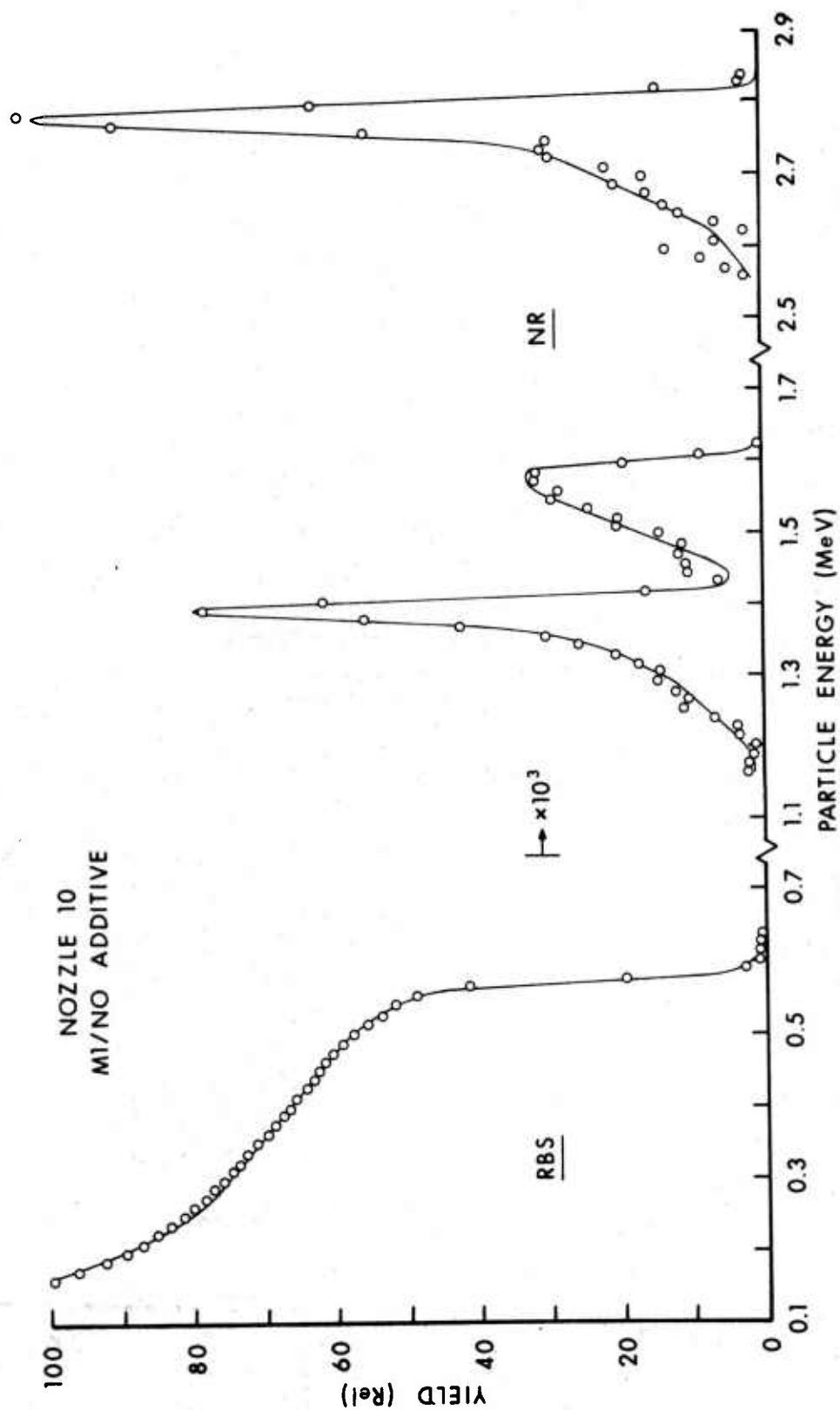
Figure 17b. Fit to the RBS and NR spectra from nozzle #10 with concentration profiles shown in figure 17(a).

Figure 18a.   Concentration depth profiles for nozzle #11.

Figure 18b. Fit to the RBS and NR spectra from nozzle #11 with concentration profiles shown in figure 18(a).

Figure 19a.   Concentration depth profiles for nozzle #12.

Figure 19b. Fit to the RBS and NR spectra from nozzle #12 with concentration profiles shown in figure 19(a).
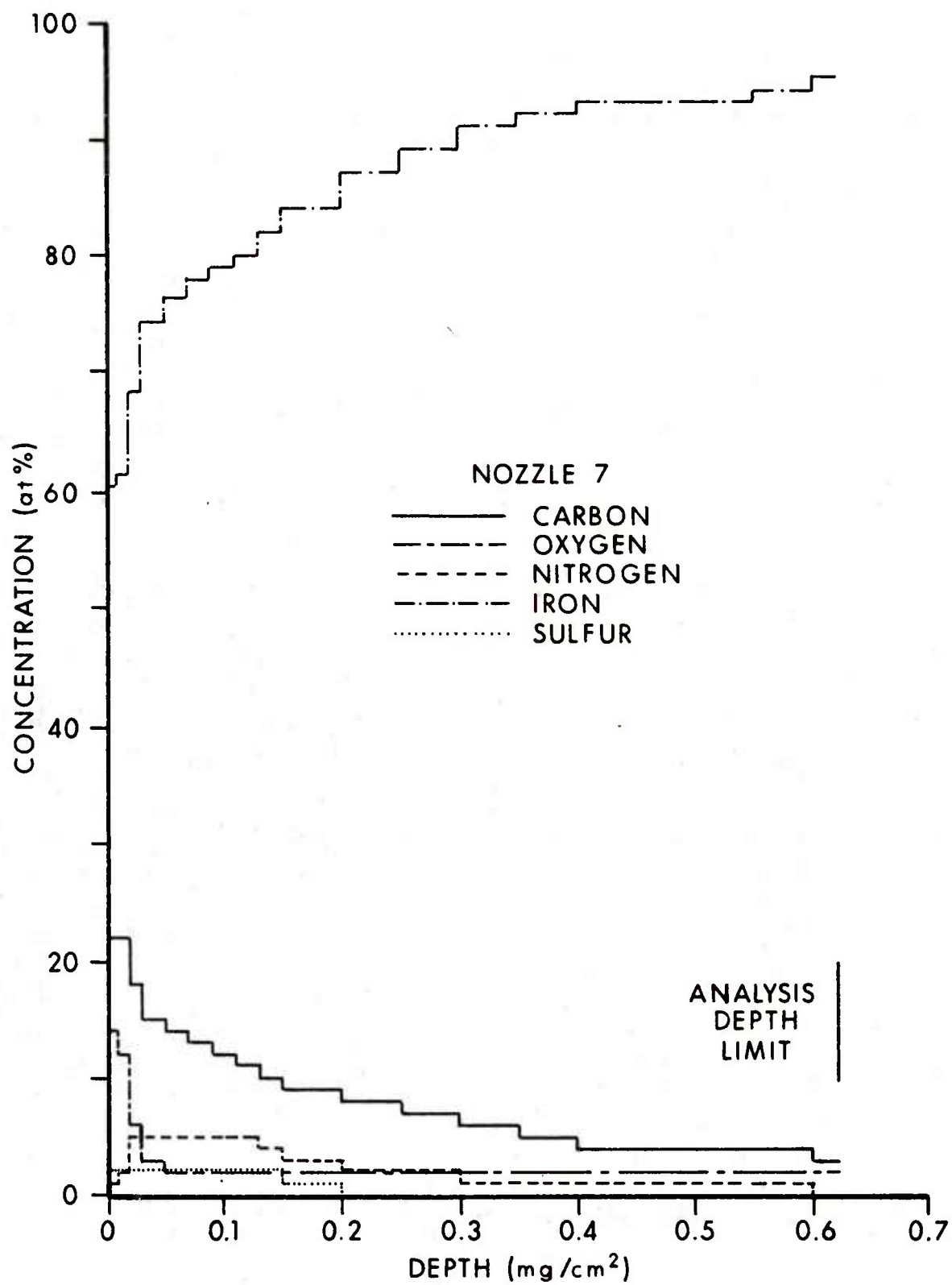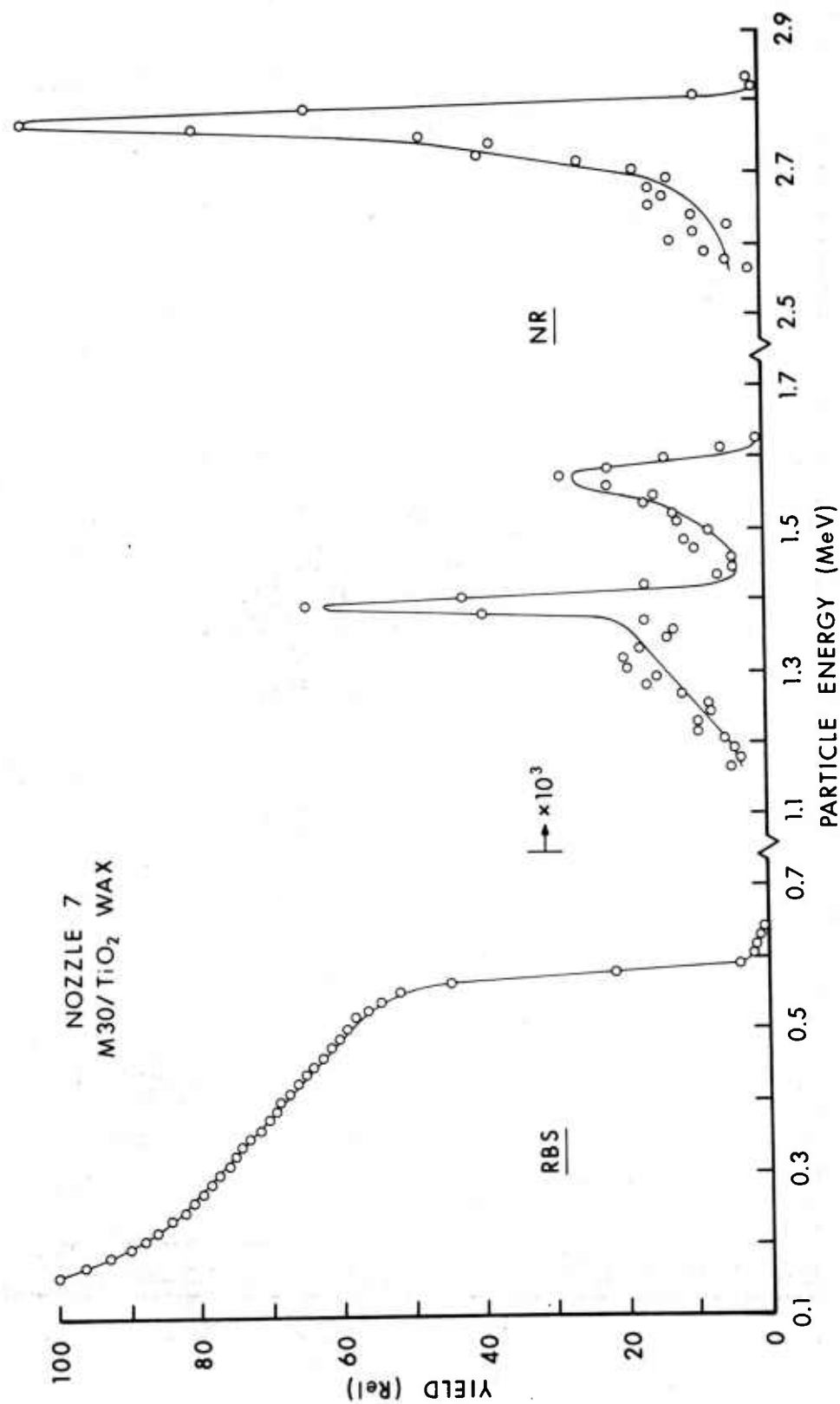
Figure 20a.   Concentration depth profiles for nozzle #13.

53

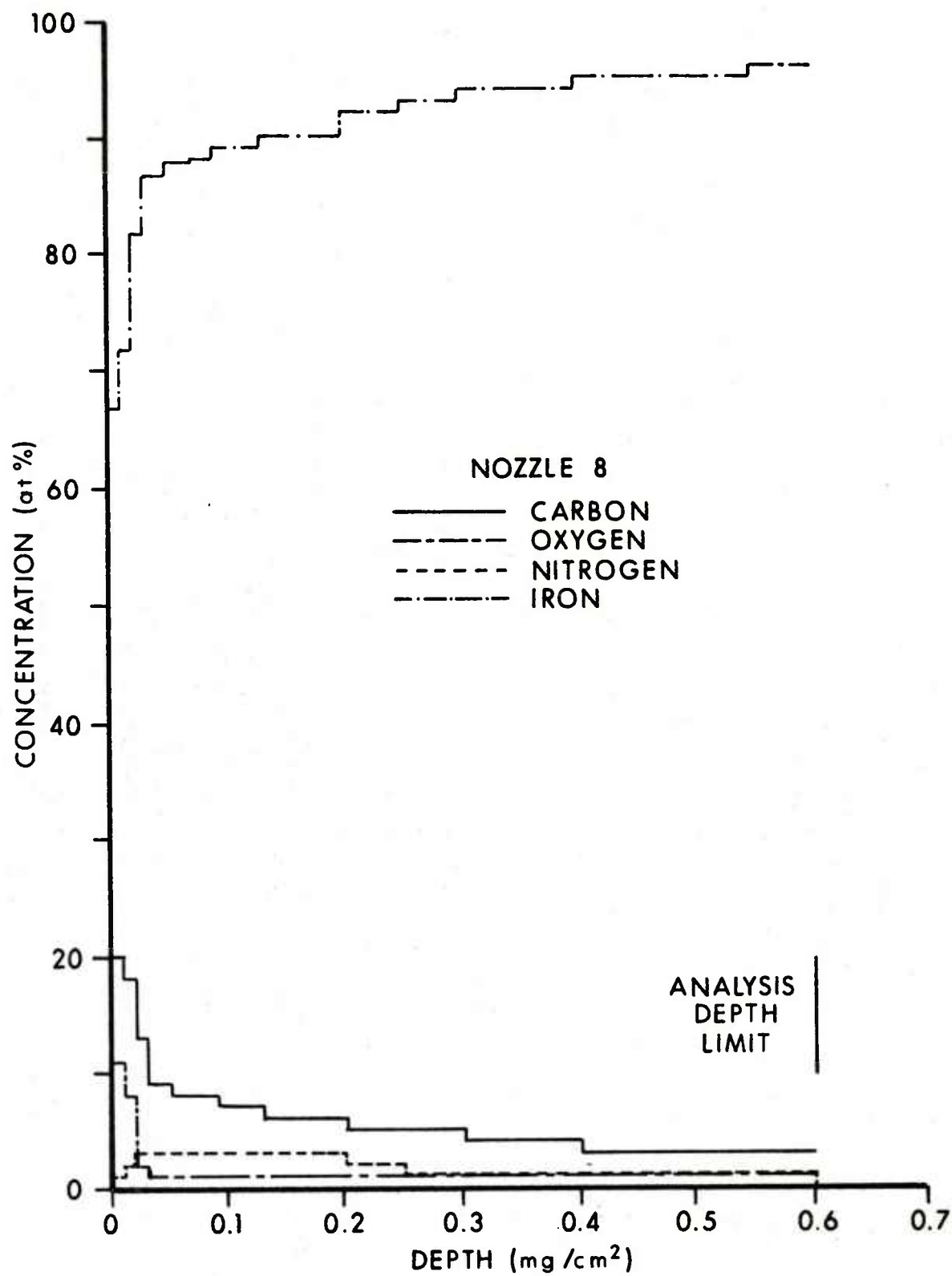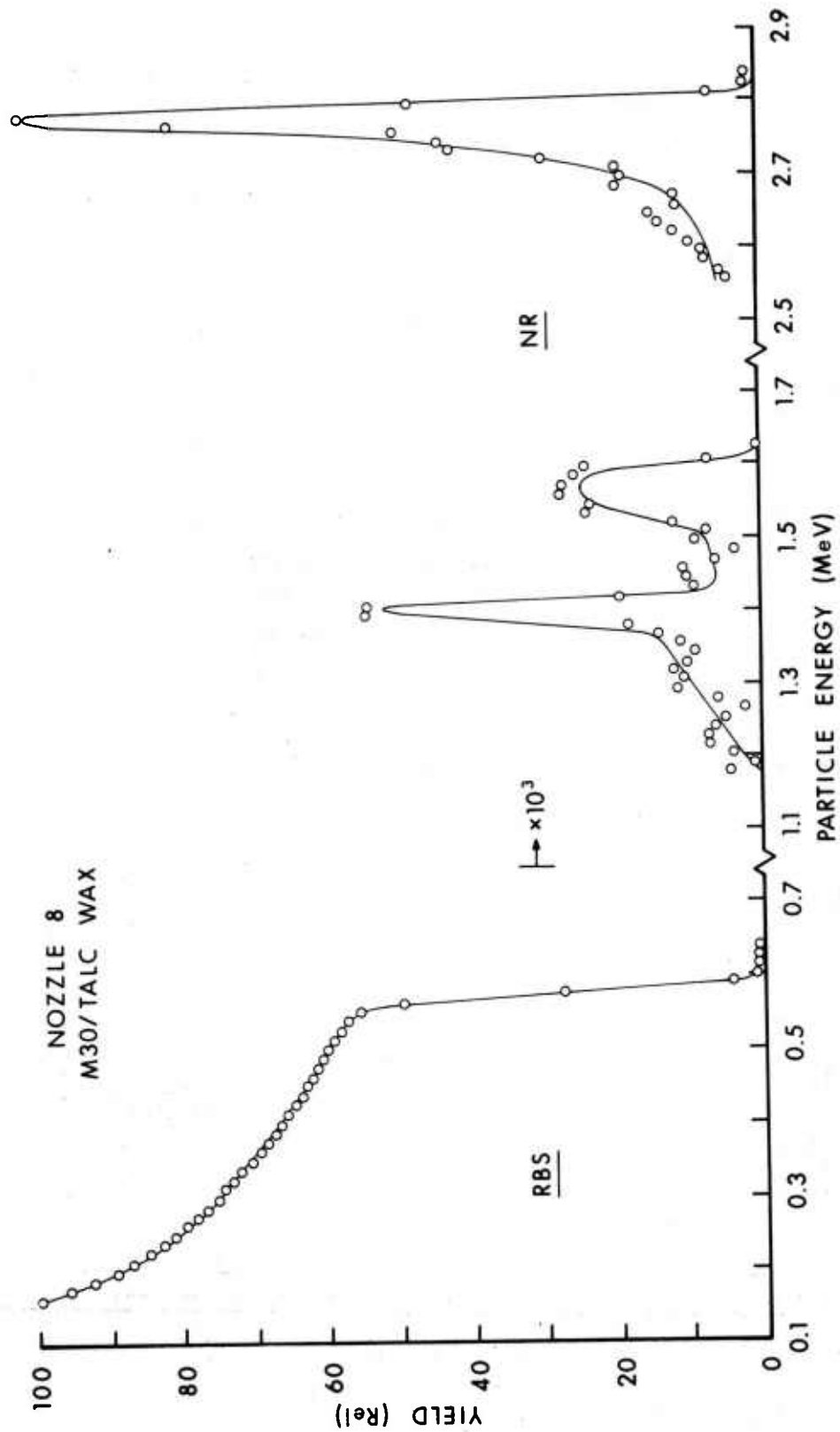Figure 20b. Fit to the RBS and NR spectra from nozzle #13 with concentration profiles shown in figure 20(a).
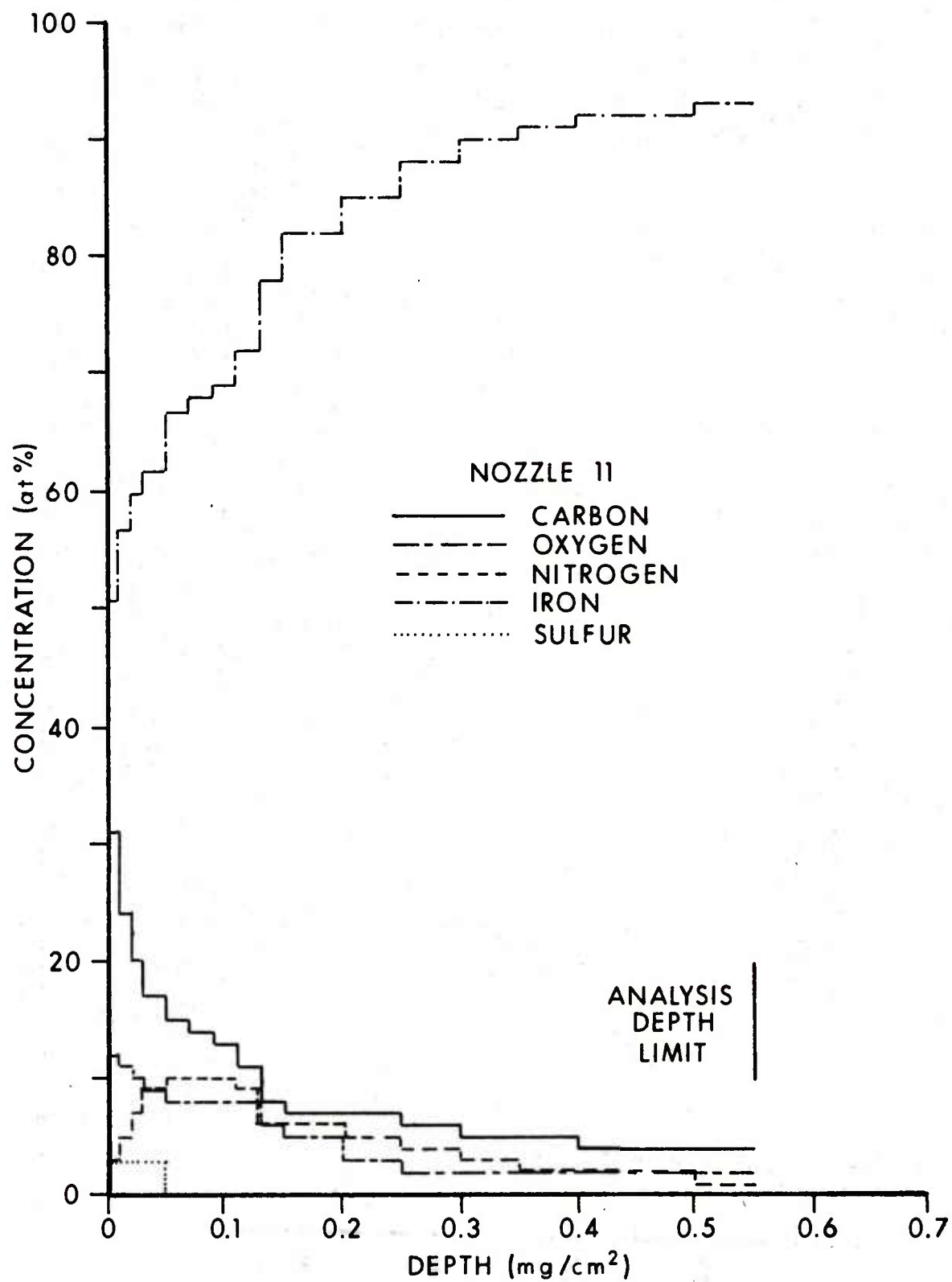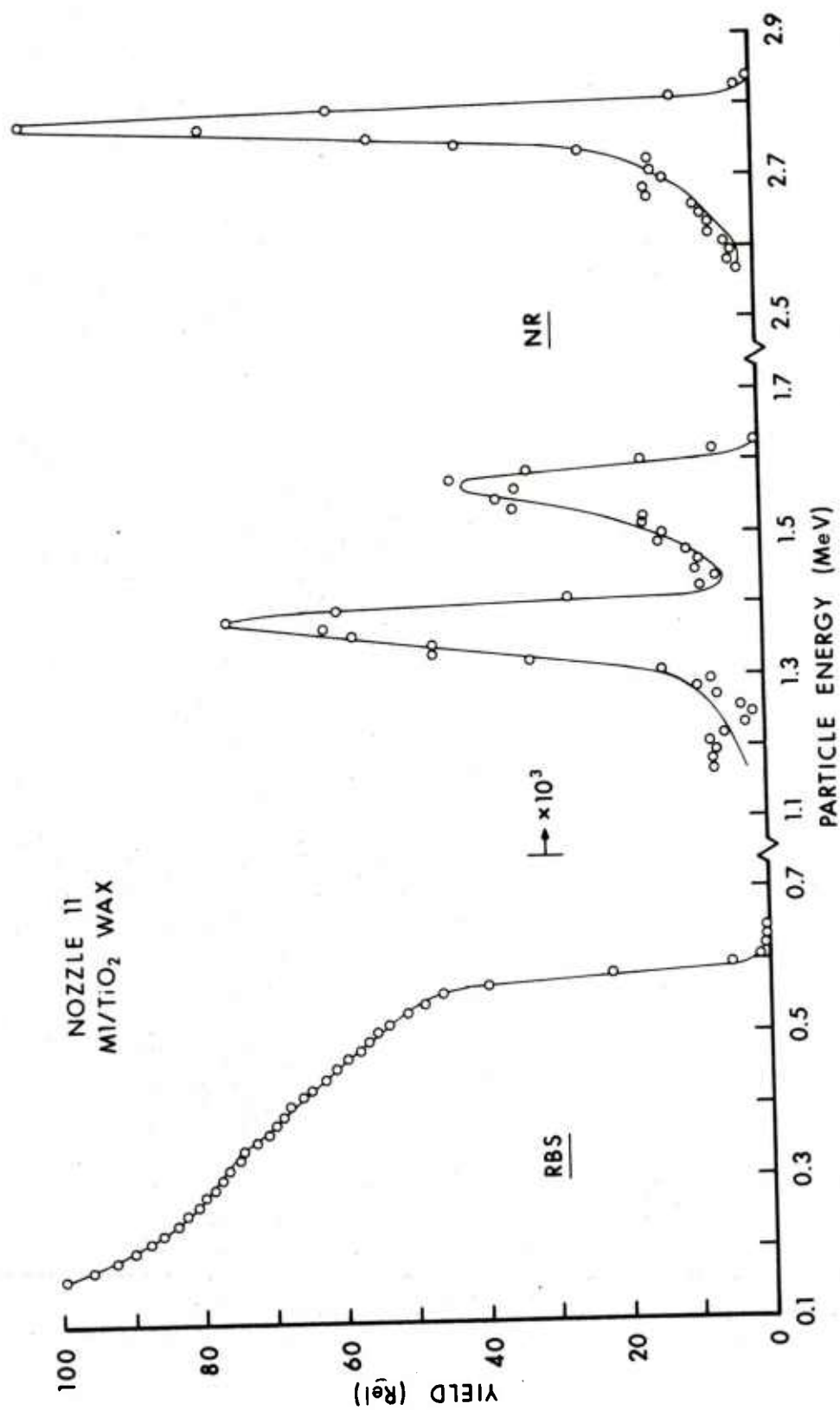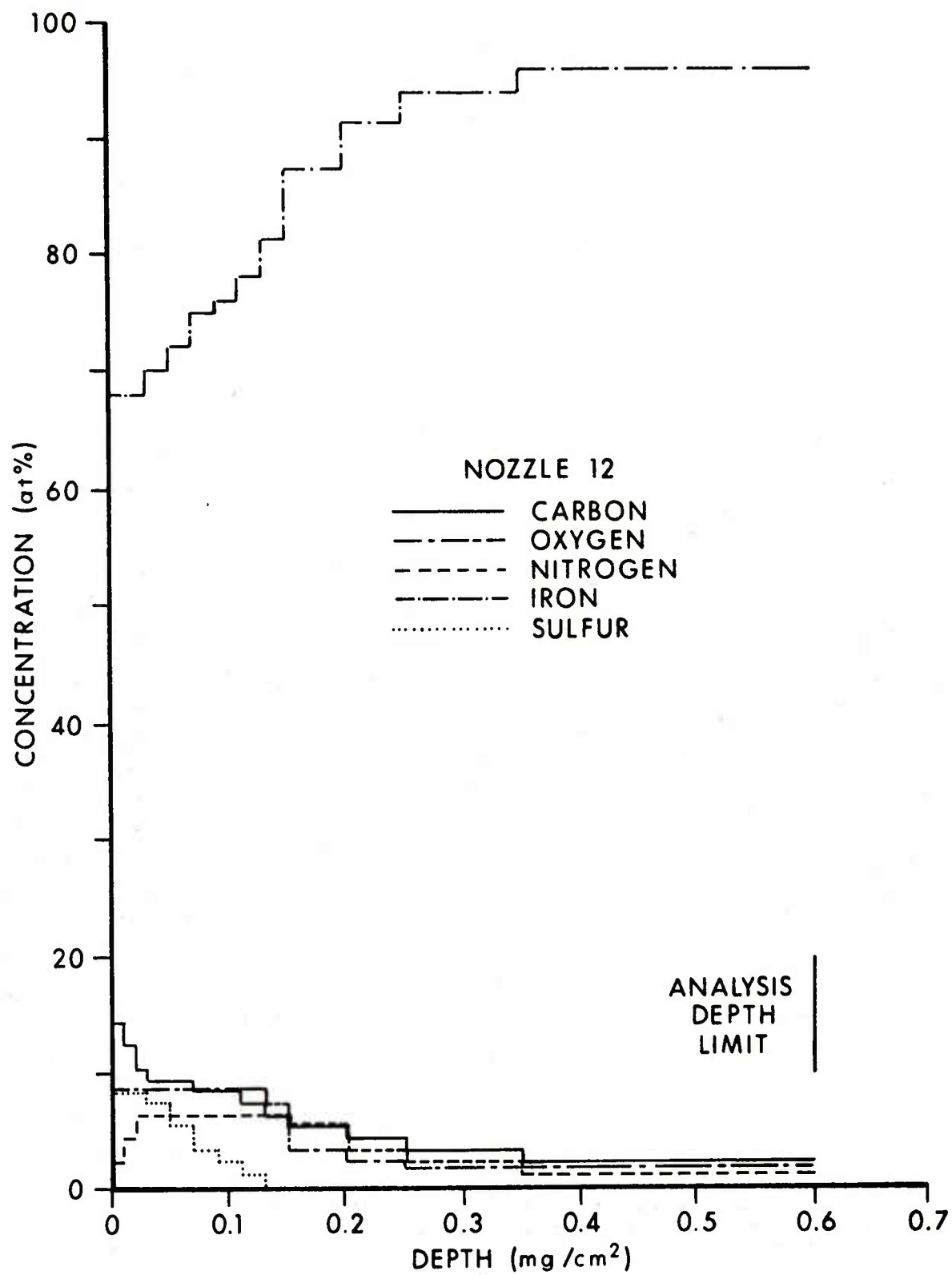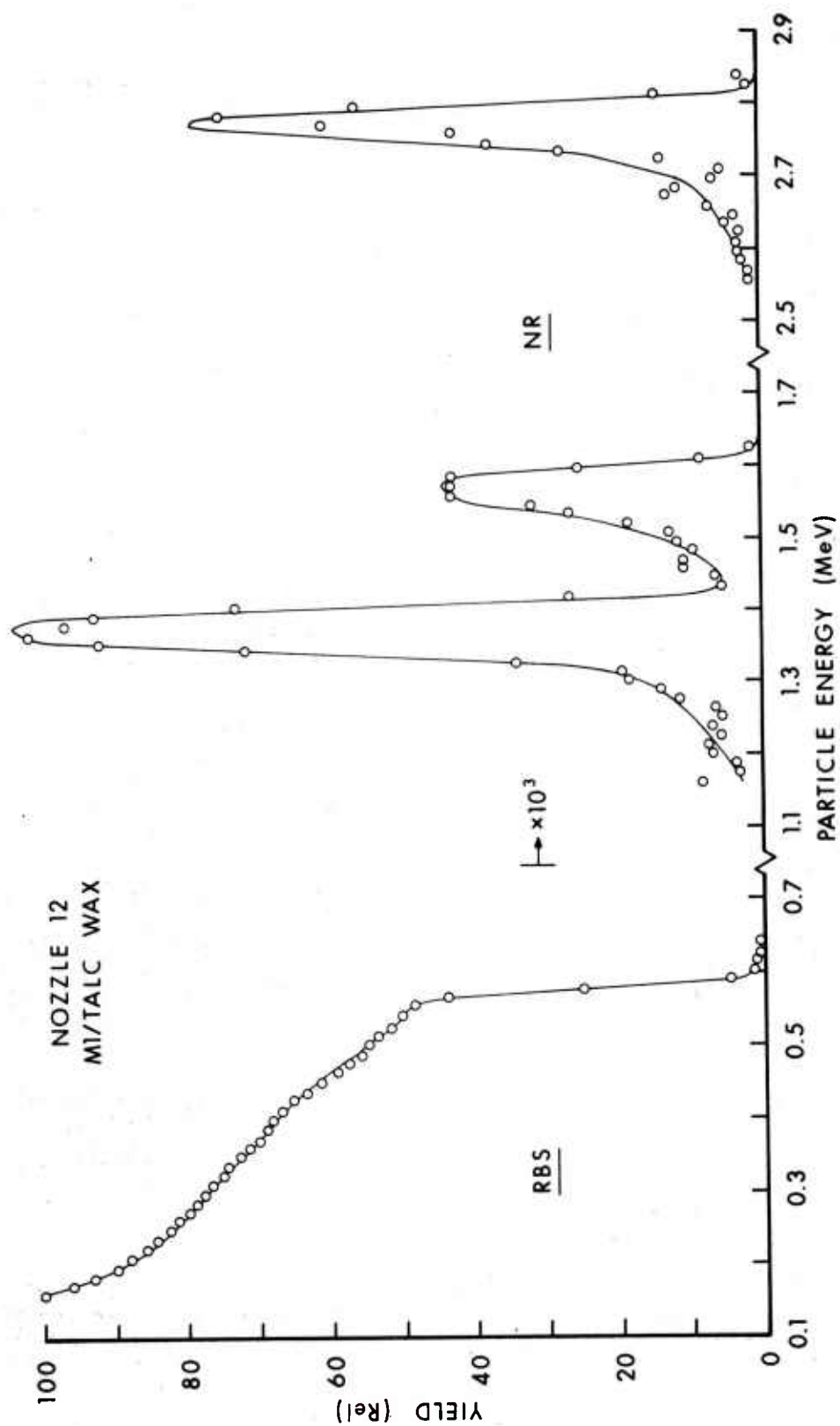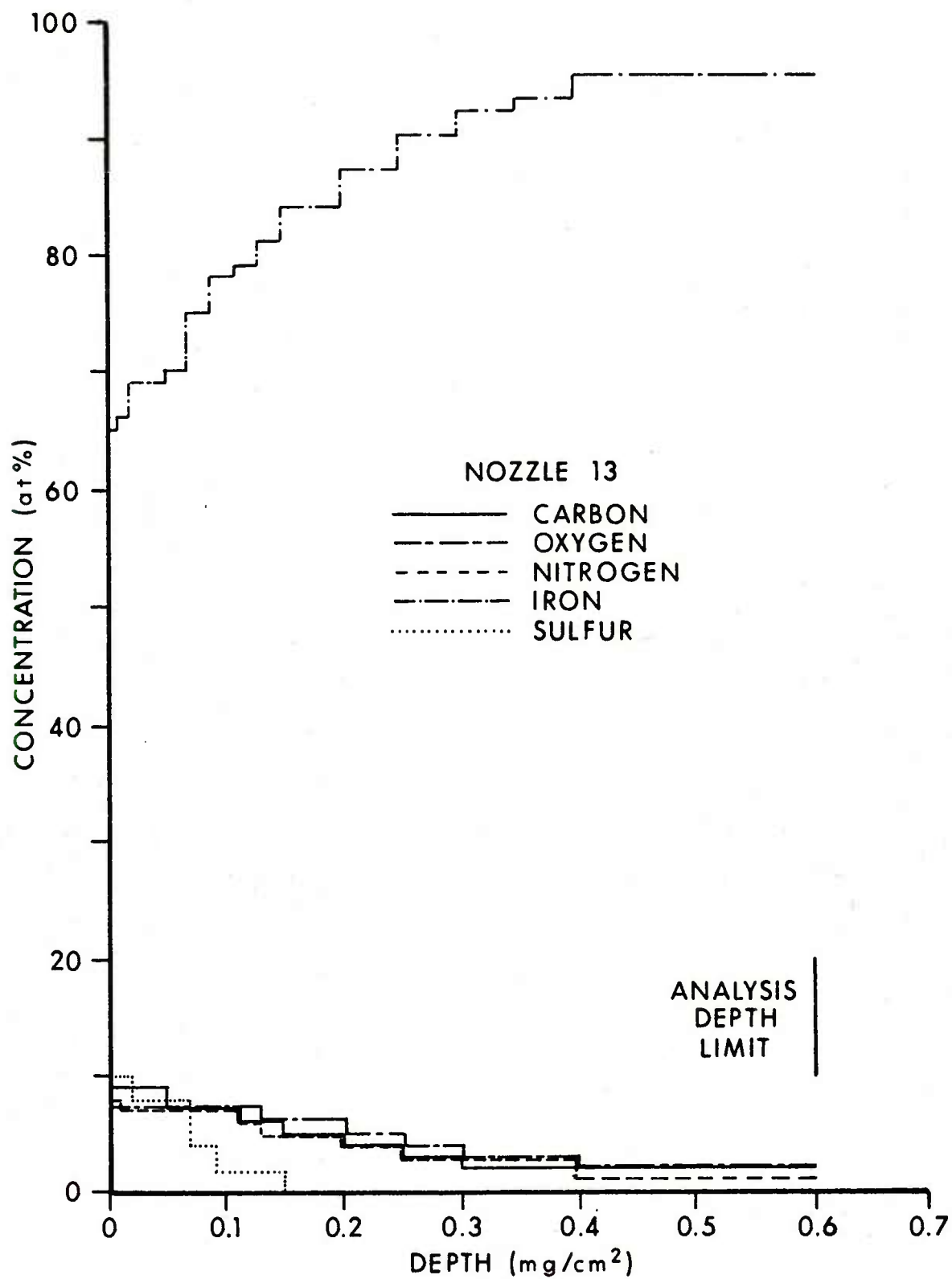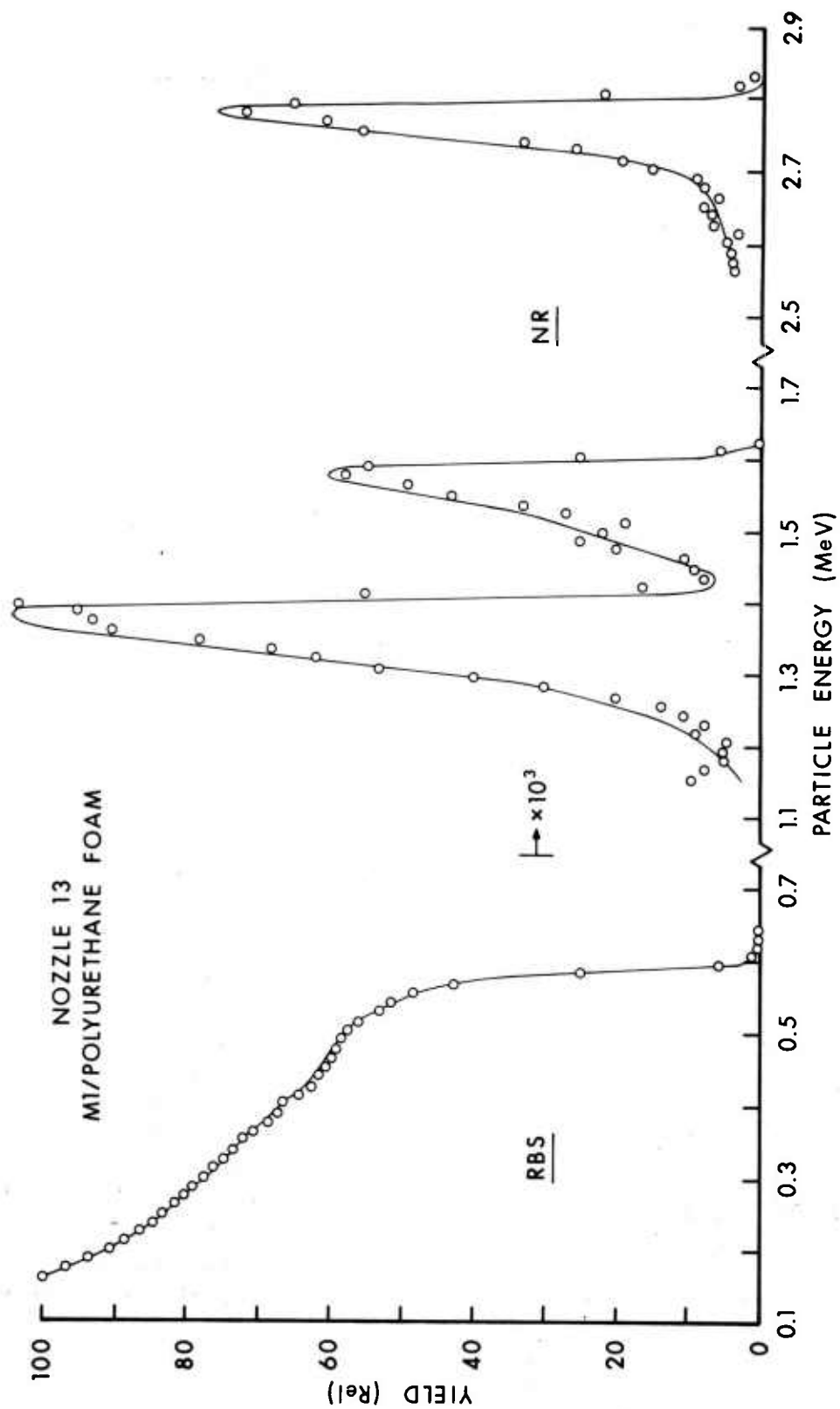
54

indicate greater concentrations. However, care should be exercised in
the latter observation because the yields as shown are relative so that
only the NR or RBS parts for a given nozzle can be compared. There is
no common scale factor between spectra from one nozzle to another. The
concentrations shown by figures 9a - 20a can, of course, be compared
with one another.

There are some common features which are observed for most of
the nozzles. Carbon, nitrogen, oxygen, sulfur and barium were observed
in most of the nozzles surfaces. The carbon and oxygen concentrations
peak at the surface for all nozzles, and drop off to relatively lower
values by the time the analysis depth limit is reached. The nitrogen
concentrations generally reach their maximum at a small distance into
the surface and then drop off to negligible values. Sulfur and Barium
are found only on the outer surface layers.

There are four possible sources of carbon on these nozzles. The
first is from the carbon used to mix with the iron to form steel and
should amount to 0.3 - 0.4%. The second carbon source is the oil which
is used to quench the steel during heat treatment. The carbon values
from the surface to the analysis depth limit are about an order of
magnitude greater than in the bulk and are due to the quenching oil. The
third source of carbon is from the burning propellant gases and the fourth
possibility is from vacuum system carbon cracking onto the outer layers
upon the surface being heated by the deuteron beam. This latter source
of carbon is most readily observed in figure 9(a) which shows a 100%
carbon peak for the outermost layer on nozzle #2. This nozzle was used
for many calibration runs, sometimes in relatively poor vacuums, so this
surface carbon peak is not surprising. In fact, visual observation shows
a dark spot where the beam hit the nozzle surface. Since it is not un-
ambiguously determinable how much observed carbon is due to heat treat-
ment or beam heat cracking, the contribution from the propellant gases
cannot be determined either. A more careful experiment in the future
using better vacuum systems and defining the carbon profile of a
virgin, unfired surface accurately would allow a better determination
of carbon content changes due to propellant gases.

Since no oxygen is allowed in the base steel, there are only two
sources for it in the nozzles. The first is simply room temperature
oxidation of the iron at the surface and the second is due to the hot
propellant gases. All nozzles show a maximum value for oxygen of ~10%
at the surface. This value agrees reasonably well with oxygen concen-
tration maxima for various steel samples and nozzles which have not been
exposed to propellants. Generally, the depth of the oxygen peak is
less than .03 $\mu g/cm^2$ for these various samples. The assumption is thus
made that all oxygen found deeper than .03 $\mu g/cm^2$ is due to the burning
propellants while it would not be possible to assign a precise source
to the oxygen found at shallower depths.

The nitrogen concentrations generally do not peak at the surface, but at a distance of .03 to .05 $\mu g/cm^2$ into the surface. Also, no nitrogen is found on unfired nozzles or other steel samples. This indicates that all nitrogen observed is due to the hot propellant gases. The reason for the small reduction in the nitrogen concentration towards the outer surface layers cannot be explained at present.

The sulfur and barium are most likely due to the $BaSO_4$ and KSO_4 found in the propellants and primers. It should be pointed out that part of what is reported as sulfur could in fact be potassium since the RBS with deuterons cannot easily distinguish between sulfur and potassium in the presence of the much larger amounts of iron and no convenient nuclear reaction peaks exist which uniquely identify these two elements. Barium concentrations were generally in the few tenths percent range and are not shown in the figures.

The concentrations of the elements C,N,O,S, and Ba, as determined by applying Eq. 4 to the analysis depth limit are given in Table 3. The uncertainties on these table values are approximately 15% as discussed in Section 3.2. From figures 9(a) through 20(a), it can be seen that in all cases, the oxygen and carbon extends at least as deeply into the surface as the analysis depth limit but in many cases, the nitrogen does not extend so far. Since all oxygen at the analysis depth limit and beyond would be expected to be introduced by the propellant exposure, there is no clear way to determine ambiguously the depth of the exposure affected layer. In order to do so, deuteron beams with higher energies should be used.

5.2 Correlations.

As the steel surfaces are exposed to the hot propellant gases, many processes can contribute to the production of the oxide/nitride layers. Some of these are absorption, adsorption, surface reactions, chemical reactions and diffusion. Since significant amounts of oxides/nitrides are found at least as deep as 7500Å (several hundred atomic layers) a mechanism such as preferential diffusion along grain boundaries is probably also present. The effects that these processes have are complicated by the presence of the shear forces of the gas flow which act simultaneously. Several correlations have been found which show evidence for two distinctly different regimes of surface erosion caused by hot gas flows.

Figure 21 shows the correlation between the O+N concentrations and the flame temperatures of the propellants. The four points at each of the temperatures represent the O+N concentrations on the nozzles fired with the different additive conditions. As can be seen, the O+N concentrations decrease with increasing temperature for all combinations. The lines are drawn to indicate the strong correlations that exist for each additive type, but are not actual fits. Except for the O+N levels

56
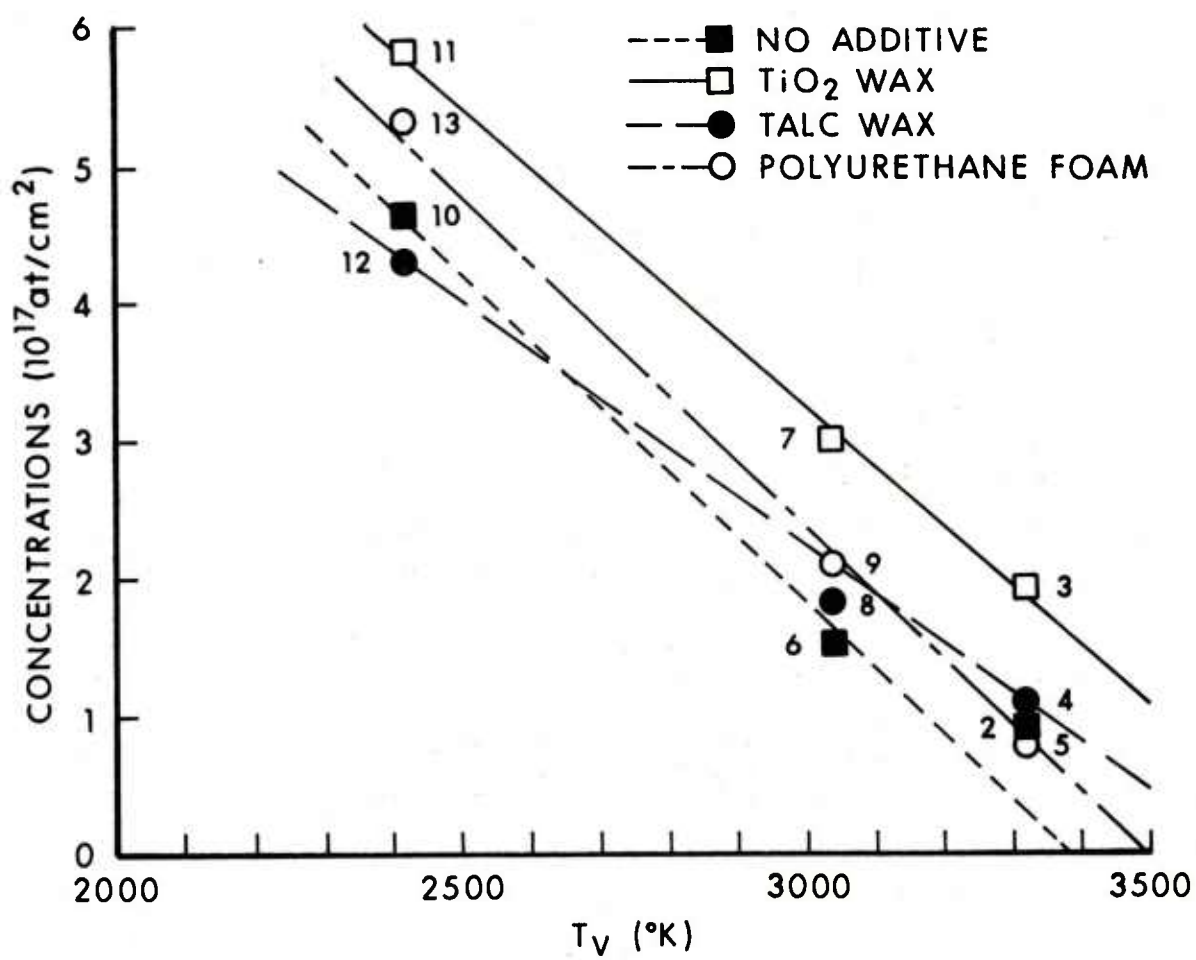
Figure 21. Correlations between O+N concentrations and the propellant flame temperatures.

Table 3. Ion Beam Analysis Results

Nozzle			Concentrations (at/cm² × 10¹⁶)			
	C	N	O(Total)	O (Subsurface)	S	Ba
2	69.5	4.1	10.9	5.5	Not observed	Not observed
3	37.1	12.3	9.0	6.8	14.0	3.5
4	24.0	4.2	10.5	6.7	2.2	1.7
5	24.2	4.6	7.0	3.3	2.0	2.7
6	28.4	8.4	8.9	6.7	7.1	2.6
7	58.1	16.1	18.5	13.8	5.8	4.8
8	38.1	11.8	9.6	6.5	Not observed	2.6
9	25.6	12.0	10.6	8.8	Not observed	1.7
10	70.1	28.9	25.0	17.5	5.6	3.2
11	59.0	33.0	30.4	25.1	2.3	3.2
12	32.6	21.4	24.9	21.6	8.1	5.2
13	28.3	25.4	30.4	27.5	10.6	2.8

are driven mainly by temperature and to a lesser extent by the additive type. Sample 2 is off the line defined by 10 and 6 because, as will be discussed later, it already has the minimum possible O+N level. Figure 22 shows the correlation between the O+N concentrations and the measured mass losses. The straight line curve shown fits nine of the data points with a correlation coefficient of 0.90. The O+N concentrations decrease with increasing wear. Figure 23 shows the correlation between the propellant flame temperatures and the mass losses. The straight line curve shown fits nine of the data points with a correlation coefficient of 0.91. As can be seen, mass loss (or wear) increases with temperature. The three data points which were excluded in the fits in figures 22 and 23 were #2, 6 and 8. The reason for this exclusion will be given later. Figures 21-23 show only the subsurface O+N concentrations.

The information presented in figures 21-23 forms the basis for the following model for erosion from this set of nozzles. All exposures produce oxygen and nitrogen layers on and in the surface of the steel. Recent work[23] shows tht the O+N concentration level for unfired nozzles is about 1×10^{17} at/cm^2. Three nozzles #2, 4 and 5 show O+N at this "background" level, #6 is barely above this "background", while all the others show significant levels above "background". Although the O+N layers may not have lower melting points, they certainly have less physical strength than bare steel and thus are more easily wiped away by the hot, flowing gases. In fact, as can be seen, the hotter exposures wear more material (see fig. 23) while leaving less of the O+N layer behind (see fig. 21). Thus it appears that the surface is "softened" and simultaneously, some of the softened layer is blown away, the amount depending on the exposure temperature. Nozzles #2, 4 and 5 appear to lose all of the O+N layers while #6 is on the borderline.

The fact that nozzle #2 is off all the correlation curves (figs. 22 and 23) suggests that something different is happening during exposure with the M2/no additive exposure. Under an optical microscope, the nozzle #2 surface appears smoother and more polished than other nozzles suggesting a melted appearance. As mentioned, this surface has no O+N levels above background and its mass loss is 3-7 times higher than from the other nozzles. This exposure is certainly the hottest of all the twelve in this experiment. A reasonable conjecture is that this exposure is hot enough so that the melting of not only the O+N layers, but also of the base steel itself can occur. Figures 22 and 23 show that nozzle #6 tends toward being off the correlations in the same way as nozzle #2 but to a lesser extent. It is possible that nozzle #6 has the second hottest exposure of all, placing it in a region where steel melting is just beginning to occur.

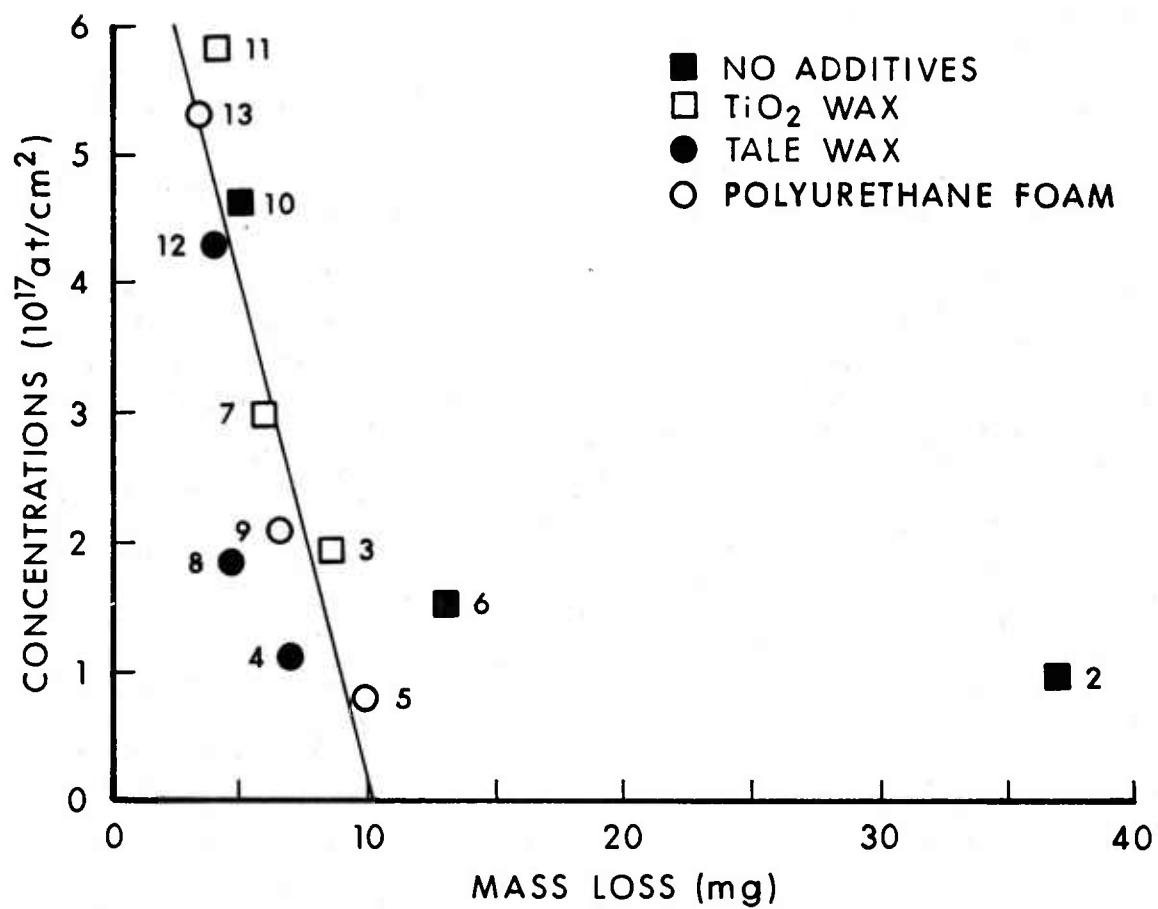---

[23] A. Niiler, to be published.

Figure 22. Correlation between the O+N concentrations and the measured mass losses.
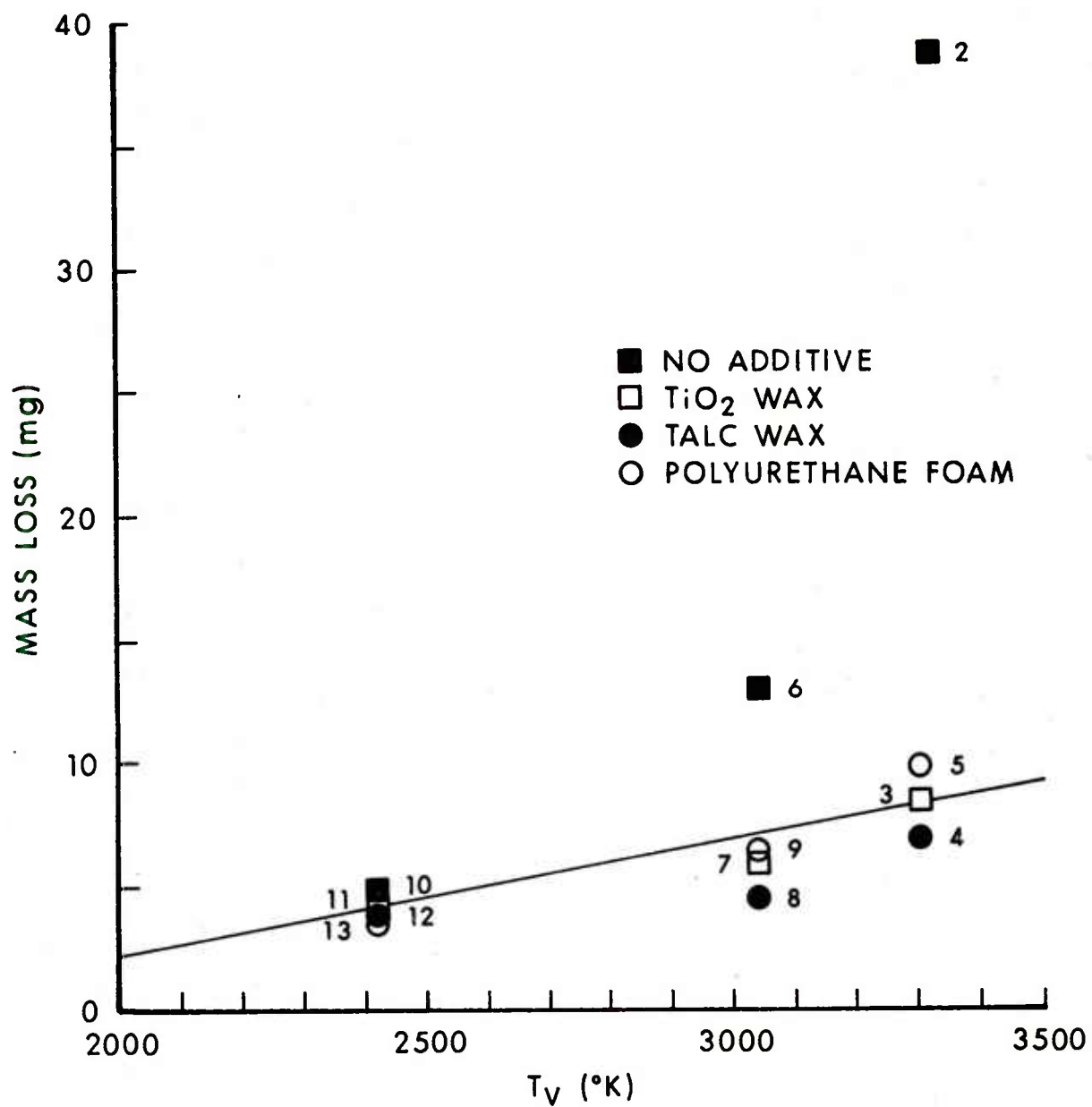
Figure 23. Correlation between the propellant flame temperatures and the measured mass losses.

The erosion mechanism indicated by the lower temperature exposures is the formation of oxide, nitride and perhaps carbon layers by physical, thermal and chemical processes followed immediately with blow-off by high temperature and velocity gas flow. We label this mechanism thermo-chemical erosion. The higher temperature exposures (nozzles 2 and 6) indicate a simpler melt and wipe-off mechanism.

The reason that the three data points from nozzles 2, 6 and 8 were excluded from the correlation fits is that they all deviated from the correlation lines much more than the average. Since the correlation lines fit the data points which describe the thermo-chemical erosion mechanism, the nozzle 2 and 6 data would not be fit if that mechanism did not apply to them. The probable reason that #8 deviates so much from the curves is that it was fired 5 times rather than 4 but the first shot was made with no blow-out disc in place. Such a significant deviation from normal shots has been found in a recent experiment[23] to affect not only concentration levels but subsequent mass losses also.

Figures 21 and 23 show possible evidence that the use of wear reducing additives do, in fact, build up non-steel surface layers which help to protect the samples against erosion. Figure 23 shows that, without exception, erosive wear is reduced whenever additives are used. Figure 21 shows that with but two exceptions, the N+O concentrations are greater whenever additives are used but those two exceptions (10/12 and 2/5) are well within experimental uncertainties of each other. The T_iO_2 wax samples show the greatest amount of residue on their surfaces even though the erosion from those samples is not significantly different from the Talc Wax or PUF samples. This fact may be important in the choice of additive under specific conditions when barrel fouling may prove a problem.

5.3 <u>Scanning Electron Microscope Observations</u>

Figure 24 shows the SEM pictures for the four nozzles 2,6,9 and 11. Figure 24a is for nozzle #2 and shows extensive cracking of the surface with the .5µ cracks running in jagged patterns suggesting grain boundaries in austentite. A similar severity of cracking is found for all the nozzles fired with M2 propellant. Nozzle #6 shows far less extensive cracking than #2 but about the same as #7, 8 and 9 which were also shot with M30 propellant. Figure 24c is taken from nozzle 9. Figure 24d, taken from nozzle #11, shows no cracks whatsoever, but does show the machining grooves have not yet been wiped away. All nozzles fired with M1 propellant show features very similar to those seen in this picture of #11. The extent of surface cracks does not correlate with the amount of wear but does correlate to the exposure temperature. The cracking is thus most likely due to the rapid thermal expansion and contraction cycling experienced by the surface.
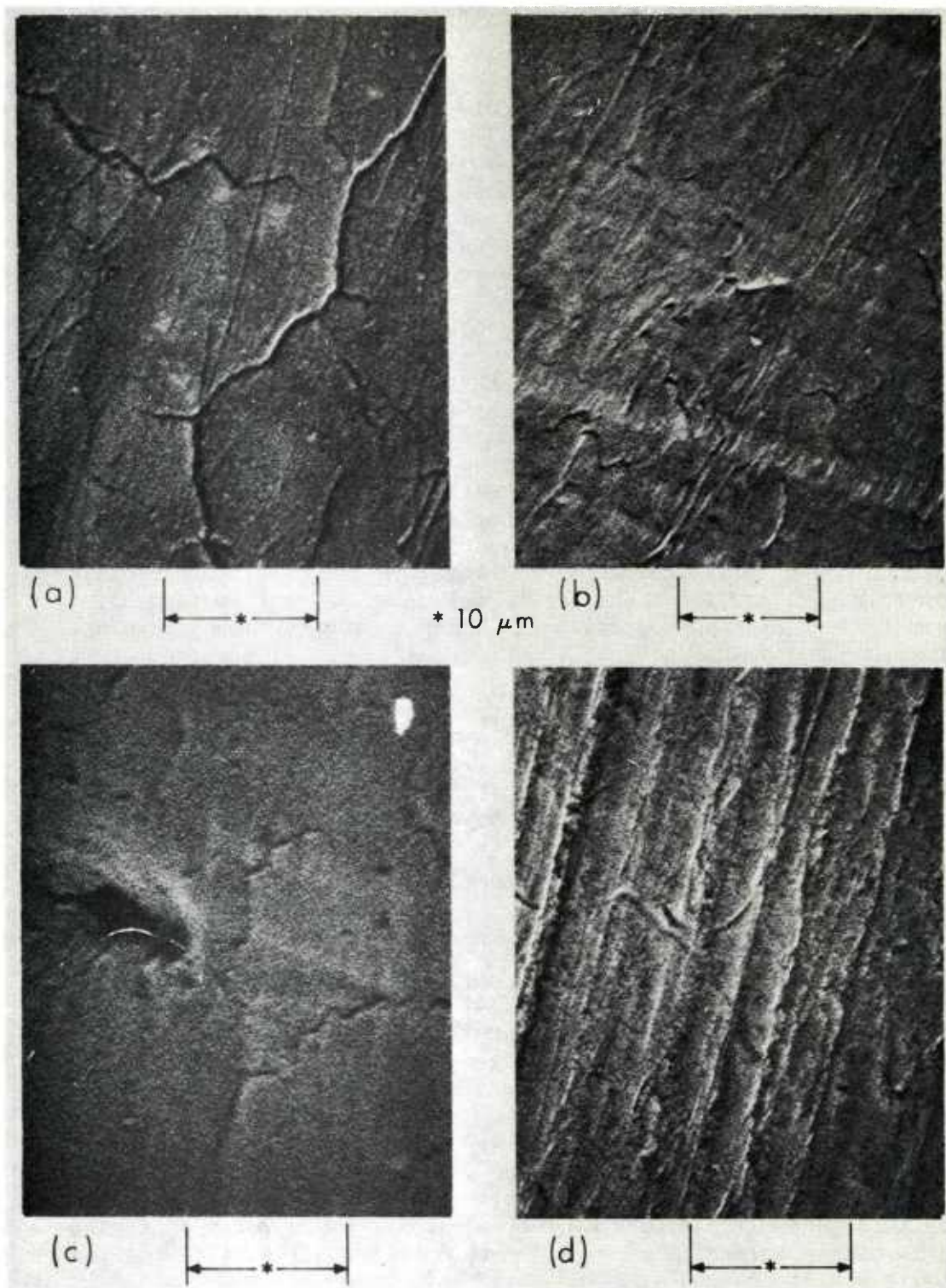
Figure 24. Scanning electron microscope photographs of the surfaces of
nozzles a) #2, b) #6, c) #9, and d) #11.

6. CONCLUSIONS

It has been shown that a method now exists which is capable of detailed characterization of atomic scale surface composition changes produced by the exposure of steel samples to propellant combustion products. This ion beam analysis method has depth resolution capability of about 0.05 μm, detectability limits in the order of 0.5 atomic percent and an absolute accuracy of about 1 atomic percent for concentrations of oxygen, nitrogen and carbon. In addition, this method is non-destructive, allowing a series of experiments to be conducted on a given sample. Most importantly, it has been shown that erosion mechanisms may now be identified from the results of such surface analyses.

The present experiment has shown that the effects of propellant burns on the surface compositions of gun steels depend strongly on propellant type (i.e. propellant flame temperature) as well as the type of wear reducing additive used. Strong correlations have been found for the total oxygen plus nitrogen concentration levels and the propellant flame temperatures as well as the amount of erosive wear observed. The flame temperatures and measured wear also correlate strongly. The analysis of the results indicate that there are at least two regimes of propellant gas erosion. The first regime, at lower temperatures, is characterized by the production of oxide/nitride surface layers and the immediate removal of part of the produced layer. The extent of the production and/or removal depends on the propellant flame temperature such that cooler propellants leave higher oxygen/nitrogen levels than the hotter ones. This mechanism is most likely thermo-chemical in nature. The second regime, at higher temperatures, is characterized by the complete absence of oxides or nitrides above background levels as well as a surface that is smooth and well polished in appearance. This mechanism is most likely surface melting and immediate wiping off of the melted material by the gas flow forces.

There are several open questions left by this work. Since the ion beam analysis is sensitive only to the atomic concentrations, no detailed chemical information can be obtained from the data. Other methods such as x-ray photoelectron spectroscopy (XPS) or secondary ion mass spectroscopy (SIMS) can be used to definitively determine the chemical forms that the observed oxygen and nitrogen are in. Such information, coupled with the present results, could then be used to better define the thermal properties of the produced layers. Any observed differences in the chemical compositions of the surface layers would lead to improved understanding of the erosive effects of individual propellants. A more precise measurement of changes in the carbon concentrations would also be important. The extent of initial and exposure related carburization is highly relevant to the strength of the steel surface and its ability to resist erosion.

ACKNOWLEDGEMENTS

REFERENCES

1. Sidney Breitbart, "On The Erosion of Metallic Nozzles by Powder Gases," Ballistic Research Laboratory Memorandum Report No. 533, April 1951.   AD #802148

2. Franklin A Vassalo and W. Richard Brown, "Shock Tube Gun Melting Erosion Study," Contract Report, ARBRL-CR-00406, August 1979. AD #A076219

3. A.C. Alkidas, S.O. Morris, C.W. Christoe, L.H. Caveny, and M. Summerfield, "Erosive Effects of Various Pure and Combustion-Generated Gases on Metals, Part II," Contract Report, AMMRC CTR 77-25, October 1977.

4. J. Richard Ward and Timothy L. Brosseau, "Role of the Insulating Layer From TiO_2-Wax Liner in Reducing Gun Tube Wear," Ballistic Research Laboratory Technical Report ARBRL-TR-02238, April 1980.

5. R. Birkmire and A. Niiler, "Applications of the Radioisotope Wear Measurement Technique," Ballistic Research Laboratory Technical Report ARBRL-TR-02075, June 1978.   AD #A058307

6. L.H. Russell, "Simplified Analysis of the Bore Surface Heat Transfer Reduction in Gun Barrels Achieved by Using Wear-Reducing Additives," Naval Surface Weapons Center Report TR-3378, October 1975.

7. "Proceedings of the Tri-Service Gun Tube Wear and Erosion Symposium," edited by Jean-Paul Picard and Iqbal Ahmad, March 1977.

8. Michael A. Schroeder and Masahiro Inatome, "The Relationship Between Chemical Composition and Wear-Reducing Effectiveness of Some Laminar Additives for Gun Propellants: Polyvinyltetrazole," Ballistic Research Laboratory Memorandum Report 2512, August 1975. AD #B007029L

9. Timothy L. Brosseau and J. Richard Ward, "Reduction of Heat Transfer in 105mm Tank Gun by Wear-Reducing Additives," Ballistic Research Laboratory Memorandum Report, BRL-MR-2698, November 1976. AD #B015308L

10. A. Niiler, J.E. Youngblood, S.E. Caldwell and T.J. Rock, "An Accelerator Technique for the Study of Ballistic Surfaces," Ballistic Research Laboratory Report No. 1815, August 1975. AD #A016899

11. A. Niiler, R. Birkmire and J. Gerrits, "PROFILE: A General Code for Fitting Ion Beam Analysis Spectra," Ballistic Research Laboratory Technical Report ARBRL-TR-02233, April 1980.   AD #A084984

12. H.H. Anderson and J.F. Ziegler, <u>Hydrogen Stopping Powers and Ranges in All Elements</u>, Pergamon Press, New York, 1977.

13. N. Longequeque, H. Beaumevieille, E. Ligeon, J.P. Longequeque, and M. Sandon, "Etude des Reactions $^{16}O(d,\alpha_o)$, $^{16}O(d,\rho_o)$ et $^{16}O(d,\rho_1)$ de 300 keV a 1 MeV (Resultats Experimentaux), Le Journal de Physique, 26, 1965, 367.

14. M. Huez, L. Quaglia and G. Weber, "Fonction D'Excitation de la Reaction $^{12}C(d, p_o)^{13}C$ Entre 400 et 1350 keV - Distributions Angulaires," Nucl. Inst. and Meth., 105, 1972, 197.

15. R.D. Edge and U. Bill, "Surface Topology Using Rutherford Backscattering," Nucl. Inst. & Meth., 168, 1980.

16. Andrus Niiler and Robert Birkmire, "Measurement of Oxygen and Nitrogen Profiles in Steel," Nucl. Inst. & Meth., 149, 1978, 301.

17. J.W. Mayer and E. Rimini, Ion Beam Handbook for Material Analysis, Academic Press, New York, 1977.

18. G. Amsel, and D. David, "Microanalysis of Nitrogen by Means of the Direct Observation of Nuclear Reactions Applications," Rev. Phys. Appl. 4, 1969, 383.

19. A. Valek, T. Vertse, B. Schlenk and I. Hunyadi, "A Study of the $^{14}N(d,p)^{15}N$ Reaction at Low Bombarding Energies," Nucl. Phys., A270, 1976, 200.

20. A. Niiler and R. Birkmire, "The $^{14}N(d,p_5)^{15}N$ Cross Section, 0.32-1.45 MeV," Nucl. Inst. & Meth., 168, 1980, 105.

21. D.L. Booth, F.V. Price, D. Roaf and G.L. Salmon, "The Differential Cross Sections for the Reactions $^{14}N(d,p)^{15}N$ and $^{14}N(d,\alpha)^{12}C$ Between 600 and 1000 keV," Proc. Phys. Soc. 71, 1959, 325.

22. V. Gomes Porto, N. Ueta, R.A. Douglas and O. Sala, "Deuteron Induced Reactions on ^{14}N," Nucl. Phys. A136, 1969, 385.

23. A. Niiler, to be published.

DISTRIBUTION LIST

No. of Copies	Organization
12	Commander Defense Technical Info Center ATTN: DDC-DDA Cameron Station Alexandria, VA 22314
1	Under Secretary of Defense Research & Engineering Office of Engineering Tech ATTN: Mr. Ray Thorkildsen Washington, DC 20301
1	Commander US Army Materiel Development and Readiness Command ATTN: DRCDMD-ST 5001 Eisenhower Avenue Alexandria, VA 22333
2	Commander US Army Armament Research and Development Command ATTN: DRDAR-TSS Dover, NJ 07801
1	Commander US Army Armament Research and Development Command ATTN: DRDAR-SC Dover, NJ 07801

4	Commander
	US Army Armament Research
	  and Development Command
	ATTN: DRDAR-LC, Dr. H. Fair
	       Dr. J. Lannon
	       Mr. C. Lenchitz
	       Dr. J. Picard
	Dover, NJ 07801

1	Director US Army ARRADCOM Benet Weapons Laboratory ATTN: DRDAR-LCB-TL Watervliet, NY 12189

No. of Copies	Organization
1	Director US Army ARRADCOM Benet Weapons Laboratory ATTN: DRDAR-LCB, Dr. I. Ahmad Watervliet, NY 12189
1	Commander US Army Armament Materiel Readiness Command ATTN: DRDAR-LEP-L, Tech Lib Rock Island, IL 61299
1	Commander US Army Aviation Research and Development Command ATTN: DRDAV-E 4300 Goodfellow Boulevard St. Louis, MO 63120
1	Director US Army Air Mobility Research and Development Command Ames Research Center Moffett Field, CA 94035
1	Commander US Army Communications Rsch and Development Command ATTN: DRDCO-PPA-SA Fort Monmouth, NJ 07703
1	Commander US Army Electronics Research and Development Command Technical Support Activity ATTN: DELSD-L Fort Monmouth, NJ 07703
1	Commander US Army Missile Command ATTN: DRSMI-R Redstone Arsenal, AL 35809
1	Commander US Army Missile Command ATTN: DRSMI-YDL Redstone Arsenal, AL 35809

DISTRIBUTION LIST

No. of Copies	Organization	No. of Copies	Organization

1	Commander
	US Army Tank Automotive
	  Research & Development Command
	ATTN: DRDTA-UL
	Warren, MI 48090
		5	Commander
			Naval Research Laboratory
			ATTN: Tech Rpt Lib
			      Dr. H. Dietrick
			      Dr. J. Hirvonen
			      Dr. C. R. Gossett
			      Dr. A. R. Knudsen
			Washington, DC 20375

2	Commander
	US Army Materials and
	  Mechanics Research Center
	ATTN: Dr. J. W. Johnson
	      Dr. R. Katz
	Watertown, MA 02172
		1	Director
			Lawrence Livermore Laboratory
			ATTN: Dr. J. Kury
			University of California
			Livermore, CA 94550

2	Commander US Army Research Office ATTN: Mr. P. Parrish Mr. E. Saibel P. O. Box 12211 Research Triangle Park NC 27709	1	Director Lawrence Livermore Laboratory ATTN: Dr. A. Buckingham University of California Livermore, CA 94550

1	Commander
	US Army TRADOC Systems
	  Analysis Activity
	ATTN: ATAA-SL, Tech Lib
	White Sands Missile Range
	NM 88002
		5	Director
			Los Alamos Scientific Laboratory
			ATTN: Dr. J. D. Seagrave
			      Dr. P. W. Keaton
			      Dr. N. Jarmie
			      Dr. S. E. Caldwell
			      Report Library
			P. O. Box 1663
			Los Alamos, NM 87544

5	Commander
	Naval Surface Weapons Center
	ATTN: Mr. M. Shamblen
	      Mr. J. O'Brasky
	      Mr. C. Smith
	      Mr. L. Russell
	      Mr. T. W. Smith
	Dahlgren, VA 22448
		3	Sandia Laboratories
			ATTN: Tech Rpts Lib
			      Dr. R. Musket
			      Dr. B. L. Doyle
			Albuquerque, NM 87115

2	Commander Naval Surface Weapons Center Indian Head Laboratory ATTN: Mr. L. Dickinson Mr. S. Mitchell Indian Head, MD 20640	1	Battelle Columbus Laboratory ATTN: Dr. George Wolken Columbus, OH 43201

2	Commander
	Naval Surface Weapons Center
	ATTN: Dr. D. Simons
	      Dr. M. Brown
	Silver Spring, MD 20910
		2	Calspan Corporation
			ATTN: Mr. G. Sterbutzel
			      Mr. F. Vassallo
			P. O. Box 400
			Buffalo, NY 14221

DISTRIBUTION LIST

No. of Copies	Organization
1	Forrestal Campus Library Princeton University ATTN: Dr. L. Caveny P. O. Box 710 Princeton, NJ 08540
2	Sony at Albany Department of Physics ATTN: Dr. W. M. Gibson Dr. W. A. Lanford 1400 Washington Avenue Albany, NY 12222
2	University of Connecticut Department of Physics ATTN: Dr. Budnick Dr. Q. Kessel Storrs, CT 06268

Aberdeen Proving Ground

Dir, USAMSAA
  ATTN: DRXSY-D
          DRXSY-MP, H. Cohen
Cdr, USATECOM
  ATTN: DRSTE-TO-F
Dir, USACSL, Bldg. E3516, EA
  ATTN: DRDAR-CLB-PA

USER EVALUATION OF REPORT

Please take a few minutes to answer the questions below; tear out this sheet, fold as indicated, staple or tape closed, and place in the mail. Your comments will provide us with information for improving future reports.

1. BRL Report Number _____

2. Does this report satisfy a need? (Comment on purpose, related project, or other area of interest for which report will be used.)

_____

_____

_____

3. How, specifically, is the report being used? (Information source, design data or procedure, management procedure, source of ideas, etc.) _____

_____

_____

4. Has the information in this report led to any quantitative savings as far as man-hours/contract dollars saved, operating costs avoided, efficiencies achieved, etc.? If so, please elaborate.

_____

_____

5. General Comments (Indicate what you think should be changed to make this report and future reports of this type more responsive to your needs, more usable, improve readability, etc.) _____

_____

_____

_____

6. If you would like to be contacted by the personnel who prepared this report to raise specific questions or discuss the topic, please fill in the following information.

Name: _____

Telephone Number: _____

Organization Address: _____

_____

_____